Variability of the cold season climate in Central Asia. Part I: weather types and their tropical and extratropical drivers

Lars Gerlitz, Eva Steirou, Christoph Schneider, Vincent Moron, Sergiy Vorogushyn, Bruno Merz

Variability of the Cold Season Climate in Central Asia. Part I: Weather Types and Their Tropical and Extratropical Drivers

LARS GERLITZ AND EVA STEIROU

Department of Hydrology, GFZ German Research Centre for Geosciences, Potsdam, Germany

CHRISTOPH SCHNEIDER

Institute of Geography, Humboldt University of Berlin, Berlin, Germany

VINCENT MORON

Aix-Marseille University, CNRS, IRD, INRA, Collège de France, CEREGE, Aix-en-Provence, France, and International Research Institute for Climate and Society, Columbia University, Palisades, New York

SERGIY VOROGUSHYN AND BRUNO MERZ

Department of Hydrology, GFZ German Research Centre for Geosciences, Potsdam, Germany

(Manuscript received 23 October 2017, in final form 22 May 2018)

ABSTRACT

To understand the atmospheric mechanisms resulting in a pronounced cold season climate variability in central Asia, an objective weather-type classification is conducted, utilizing a *k*-means-based clustering approach applied to 500-hPa geopotential height (GPH) fields. Eight weather types (WT) are identified and analyzed with regard to characteristic pressure patterns and moisture fluxes over Eurasia and specific near-surface climate conditions over central Asia. To identify remote drivers of the central Asian climate, WT frequencies are analyzed for their relationships with tropical and extratropical teleconnection modes. The results indicate an influence of Northern Hemispheric planetary wave tracks on westerly moisture fluxes with positive anomalies of precipitation associated with the formation of a Rossby trough over central Asia. Particularly the propagation of the east Atlantic–western Russia and the Scandinavian patterns is shown to modulate regional climate conditions. Variations of ENSO are shown to affect the frequency of particular WTs because of the formation of an anticyclonic anomaly over the Indian Ocean and an increase of tropical fluxes of moisture and heat into central Asia during El Niño events. Further a WT internal influence of ENSO is distinctly defined, with enhanced moisture supply during the ENSO warm phase. The analysis of climatic trends shows that 50% of observed temperature changes can be assigned to variations of the WT composition, indicating that most likely changing regional circulation characteristics account for the enhanced warming rates in central Asia. Trends of precipitation sums are likewise shown to be associated with changing WT frequencies, although the WT–precipitation relationships include large uncertainties.

1. Introduction

Central Asia, comprising Kazakhstan, Kyrgyzstan, Uzbekistan, Tajikistan, Turkmenistan, and Afghanistan, is characterized by a highly continental climate. More than half of the annual precipitation falls as snow during the extended winter season (November–March, or cold season), particularly in cold mountain regions, and is released in the subsequent spring and summer, allowing the irrigation of the vast cultivated areas along the Syr Dar'ya and Amu Dar'ya river systems (Barlow and Tippett 2008; Schär et al. 2004; Schiemann et al. 2008; Apel et al. 2018). Thus, cold season precipitation anomalies, and also slightly negative precipitation trends during recent decades as reported by Palazzi et al. (2013), Golian et al. (2015), and Barlow and Hoell (2015), significantly affect the rural economies of the riparian areas. Regional warming, which exceeds the global average (Chen et al. 2009), results in an increase of evapotranspiration and a decrease of glacier coverage and thus further intensifies

Corresponding author: Lars Gerlitz, lars.gerlitz@gfz-potsdam.de

DOI: 10.1175/JCLI-D-17-0715.1

water-related challenges (Duethmann et al. 2015; Bhandari and Panthi 2014; Barnett et al. 2005).

In general, the climate of central Asia is influenced by westerly circulation patterns and associated moisture fluxes throughout the year. Precipitation during the boreal cold season is mainly triggered by midlatitude disturbances originating from the Atlantic Ocean and the Mediterranean and by the uplift of the westerly flow at high mountain barriers, such as Tian Shan, Pamirs, and Karakoram Range (Bohner 2006; Bothe et al. 2012; Gerlitz et al. 2015; Maussion et al. 2014). The track of westerly disturbances as well as the trajectories of large-scale moisture fluxes are connected with the position of the westerly jet stream at the polar frontal zone leading to a distinct seasonal cycle of precipitation. The southern parts of central Asia, particularly the windward slopes of the Karakoram and Hindu Kush mountain ranges, receive high amounts of winter precipitation (December-January-February), which reaches up to 60% of the total annual precipitation (Bohner 2006; Gerlitz et al. 2015; Wulf et al. 2010). During spring the zone of maximum precipitation migrates northward, reaches the Pamirs in March, and continues to Tian Shan in April/May. Mariotti (2007) illustrates that a northward current over the Arabian countries transports tropical air masses from the Arabian Gulf into central Asia, which interact farther north with the westerly background flow and represent an important additional moisture source. The interannual variability of winter and spring precipitation in central Asia has been frequently related to variations of El Niño–Southern Oscillation (ENSO). Severe droughts (e.g., 1989, 1999–2001, 2008) have been linked to the contemporaneous El Niño cold phase (La Niña; Barlow et al. 2002, 2016; Hoell et al. 2014; Gerlitz et al. 2016). Statistically significant correlations of winter precipitation anomalies over the Karakoram Range and Himalayas with contemporaneous ENSO indices have been reported by Dimri (2013) and Yadav et al. (2010). Roghani et al. (2016) and Shirvani and Landman (2016) found strong correlations of winter precipitation amounts over Iran with the Southern Oscillation index (SOI) during the preceding summer and autumn. Mariotti (2007), Trigo et al. (2010), and Dimri (2013) illustrate that ENSO variations alter the intensity of tropical moisture fluxes into central and South Asia. The El Niño warm phase is associated with simultaneous positive pressure anomalies over the western Indian Ocean, resulting in a weakened Hadley cell, and hence increased moisture fluxes into the target region. On the contrary, La Niña promotes an anticyclonic anomaly over central Asia, resulting in precipitation-suppressing subsidence. A similar mechanism has been proposed by Barlow et al. (2002), taking the sea surface temperature (SST) of the Indo-Pacific warm pool (which is highly anticorrelated with ENSO) as a covariate. Their results suggest a teleconnection between warm pool SST anomalies and Northern Hemispheric planetary wave tracks. Barlow and Hoell (2015) argue that increasing warm pool SSTs might be responsible for recent negative precipitation trends in the Middle East and southwest Asia, although a direct attribution is not yet confirmed.

Besides tropical SST modes, the impact of contemporaneous wave patterns over the Atlantic and Eurasian domain on the winter climate of central Asia has been frequently addressed. Schiemann et al. (2008, 2009) illustrate that an anomalous location or strength of the westerly jet stream results in a modified precipitation pattern over central and high Asia. Dimri (2013) shows that moist winter conditions over the Karakoram Range and the Himalayas are associated with a southward shift of the westerly jet stream. Bothe et al. (2012) demonstrate that dry and moist winter seasons over the Tian Shan are dominated by different planetary wave tracks and the relative position of the orographic barriers to the westerly flow. Significant correlations of winter precipitation sums with well-known Euro–Atlantic circulation modes, such as the North Atlantic/Arctic Oscillation (NAO, AO), and the east Atlantic (EA), Scandinavian (SCA), polar–Eurasian (POL/EUR), and east Atlantic–western Russia (EA/WR) patterns have been detected. Syed et al. (2006, 2010) show that enhanced winter rainfall over Afghanistan, Pakistan, Tajikistan, and Uzbekistan is triggered by El Niño and intensified westerlies during the positive phase of NAO. Bastos et al. (2016) illustrate that moisture fluxes into central Asia are controlled by a combined influence of the NAO and the EA pattern. The latter has been shown to be strongly correlated with ENSO indices (Iglesias et al. 2014) impeding the investigation of its independent influence. Yin et al. (2014) further highlight the effect of the EA/WR and POL/EUR patterns on the central Asian winter climate. Enhanced moisture fluxes are associated with the positive phases of both circulation modes. Finally, the tropical stratospheric quasi-biennial oscillation (QBO) has been shown to significantly influence the precipitation climate over vast parts of Asia. Observations show that the positive phase of QBO (corresponding to westerly winds in the tropical stratosphere) is associated with a stronger and zonal-oriented polar vortex, which favors a positive state of AO with negative geopotential height (GPH) anomalies and enhanced westerly moisture fluxes over Eurasia (Boer and Hamilton 2008).

While the influence of large-scale teleconnections on the economically relevant hydroclimatic variations over central Asia has been addressed by several studies, temperature-related investigations mainly focus on long-term changes and the consequential impacts. Central Asia has been identified as one of the hot spots of global warming with warming rates of up to 0.23°C decade^{-1} during the past century (Chen et al. 2009; Giorgi 2006), and projected temperature changes up to +4.8°C during the twenty-first century exceed the global average (IPCC 2013).

Whether the enhanced warming is due to changes of the large-scale or regional circulation, which might reflect interannual or decadal variations of natural climatic modes, or due to intensified thermodynamic changes, for example, because of regional climate change feedback mechanisms, remains unclear. The investigation of the interannual temperature variability in central Asia and the role of large-scale circulation modes has rather been neglected so far.

From a methodological perspective, the investigation of teleconnections based on the statistical relation of large-scale circulation indices with surface variables raises questions because of large inherent uncertainties. This is due to the quality and the short period of available observations (particularly in data-scarce regions such as central Asia) that often result in a lack of statistical significance and spurious correlations. Thus, the influence of large-scale atmospheric modes on the regional-scale circulation and the underlying atmospheric processes linking remote teleconnection indices with observed climate anomalies are often not well understood (Lee 2017). The analysis of discrete weather types (WT), representing an intermediate scale between the large-scale circulation and the regional climatology, has been used to address this physical link for various target regions (e.g., Sheridan 2003; Coleman and Rogers 2007; El Kenawy et al. 2014; Liu et al. 2016). Therefore WTs are derived by means of a subjective categorization or an objective, that is, data-driven, classification of regional pressure fields (Philipp et al. 2010).

To bridge the scale gap between large-scale teleconnection indices and observed climate anomalies in central Asia, we here present what appears to be the first objective weather-type classification for this region. We therefore employ a *k*-means-based optimization algorithm (Philipp et al. 2010) to regional GPH fields. An overview of the applied WT classification technique is given in section 2. The WT classification allows the identification of synoptic regimes and a detailed investigation of the regional-scale circulation. WTs are systematically analyzed with regard to their associated large-scale manifestation of pressure patterns and moisture fluxes over Eurasia as well as their typical spell lengths and transitions in sections 3a and 3b. Northern Hemispheric circulation indices and tropical climate modes are related to the frequency of WTs, allowing a detailed assessment of the influence of tropical and extratropical drivers on the regional-scale circulation over central Asia (section 3c). With the aim of identifying the atmospheric mechanisms resulting in observed surface climate anomalies during the boreal cold season, the spatial temperature and precipitation characteristics are investigated for each WT in section 3d. Eventually the interannual variability and change of WT frequencies is tested for its skill to explain variations and trends of seasonal mean temperatures and precipitation sums in central Asian subregions. Section 4 gives a brief summary of the findings, and section 5 discusses the applicability of the results for climate change investigations and seasonal forecasting approaches. In a follow-up study (Part II), we will focus on the latter, particularly by investigating the lagged relationships between seasonal WT frequencies and the state of tropical and extratropical predictor variables.

2. Data and methods

a. WT classification methodology

We conduct a weather-type classification based on 6-hourly 500-hPa GPH fields of the ERA-Interim reanalysis (Dee et al. 2011) for the boreal cold seasons from 1979 onward. Because of the integration of dynamical atmospheric modeling and data assimilation, ERA-Interim serves as a best guess of large-scale atmospheric conditions and has been positively evaluated for central and high Asia at various temporal and spatial scales (Bao and Zhang 2013; Wang and Zeng 2012). The 500-hPa level is chosen for the analysis, since it captures the free atmospheric circulation over the entire target region, except of single mountain peaks. Further, it represents near-surface climate conditions over the hydroclimatologically relevant mountain ranges. A domain covering central Asia as well as western China and northern India (20°–60°N, 50°–90°E) is selected in order to capture the major large-scale features of the wintertime circulation, with regard to the southward shift and division of the polar frontal jet stream into a northern branch over southern Russia and a southern branch along the Himalayan arc (Bohner 2006; Gerlitz et al. 2015).

Assuming that the regional atmospheric circulation over the target region tends to adopt a number of characteristic states, we conduct a *k*-means cluster analysis of GPH fields utilizing an approach proposed by Michelangeli et al. (1995) and modified by Roller et al. (2016). GPH fields are standardized by mean and standard deviation ensuring a similar influence of each grid cell on the final cluster solution, irrespective of the magnitude of absolute GPH variations. This leads to a similar footprint of northern and southern parts of the target region, although the north is characterized by a strong seasonal cycle of GPH, with higher GPH values in November and a successive penetration of lower pressure due to a southward shift of the polar frontal zone, while the south exhibits more stable values throughout the year. The seasonality is not removed in order to identify WTs characterizing both the seasonal cycle and intraseasonal variations of the regional circulation. Normalized GPH fields serve as an input for an empirical orthogonal function (EOF) analysis and the scores of EOF modes amounting to 95% of the total variance are used as input for the k-means cluster analysis. The EOF-based data transformation reduces the computational demand of the classification algorithm and serves as a spatiotemporal filter, eliminating small-scale and erratic GPH variations, such as individual low pressure systems and moving cyclones. The WT classification is based on the dynamical k-means cluster algorithm (Diday and Simon 1980). However, k-means clustering faces two shortcomings when applied to WT analysis. First, the iterative procedure might converge to a solution that does not represent the best separation of the GPH data, since the clustering depends on randomly distributed initial seeds. Second, the algorithm requires a subjective definition of the number of clusters. Both points are addressed by a repeated execution of the k-means approach and a subsequent estimation of a classifiability index, which quantifies the robustness of the cluster solutions. For a number of clusters ranging from $k = 2$ to 20, 100 cluster realizations are computed and results are compared by means of an anomaly correlation analysis. For each combination of two independent cluster solutions with k classes, the anomaly correlation coefficient (ACC) serves as a measure of similarity of the considered realizations, with ACC = 1 indicating complete equality. An ACC score is assigned to each realization as the mean of ACC values of the particular cluster solution and all other realizations with the same number of classes. For each number of k, the cluster solution with a maximum ACC score is considered as the best separation of the data. Michelangeli et al. (1995) show that the procedure eliminates the influence of randomly selected cluster seeds and generates robust and reproducible cluster solutions. To identify an optimum number of clusters for the weather-type classification, a classifiability index (CI) is defined as the mean of ACC scores for each number of k. CI values near 1 indicate that the k-means partition is rather unaffected by cluster seeds and thus data are well classifiable into k clusters. For the estimation of CI significance, we conduct the same analysis for 100 red-noise records with equal statistical characteristics. The artificial records are derived based on a first-order autoregressive model (ARIMA) retaining mean, standard deviation, and lag-1 autocorrelation of the original data. The CI is calculated based on 100 cluster realizations for each of the records and for each value of k. A two-sided confidence interval of CI values is constructed based on the 5% and 95% quantiles of the red-noise-based CI distribution. The original GPH fields are assumed to be significantly better classifiable into k clusters than the artificial records if the corresponding CI value exceeds the upper bound of the confidence interval for a given k. Since CI values tend to continuously increase with rising k, the optimum number of clusters is usually defined as the lowest k with a significant CI value. For a detailed delineation of the anomaly correlation coefficient and the classifiability index, the reader is referred to Michelangeli et al. (1995) and Roller et al. (2016).

b. *Large-scale manifestation, transitions, and drivers of WT*

The derived WTs are analyzed with regard to their mean frequencies at seasonal and monthly scales, making it possible to delineate the seasonal cycle as well as intraseasonal variations of the regional circulation. To identify large-scale circulation patterns related to the occurrence of WTs, composite maps of 500-hPa GPH and vertically integrated moisture fluxes as well as vertically integrated moisture divergence are depicted for all of Eurasia. The spatial distribution of anomalies is analyzed for each large-scale variable, and significant deviations from the seasonal mean are tested based on a 100-fold bootstrap resampling of random WT sequences. Although this approach does not retain observed WT spells, as would be the case for a reshuffling of WT blocks, we assume that the significance of anomalies is not affected.

With the aim of identifying typical WT sequences, WT transitions are analyzed for lag times of 3, 5, 7, and 9 days, respectively. Observed transitions are compared with a random permutation of the WT time series in order to detect WT successions with significantly increased frequencies. Further, the WT distribution 3, 5, 7, and 9 days after the end of a WT spell is depicted for each WT, making it possible to deduce frequently occurring WT passages. The proportion of spells lasting longer than 3, 5, 7, and 9 days is computed for each WT in order distinguish between types with short duration (which might reflect a transient state of the regional circulation) and persistent types.

The influence of large-scale atmospheric modes on the frequency of WTs over central Asia is analyzed with regard to well-known teleconnection indices. We consider Northern Hemispheric circulation indices, such as the NAO and AO and the EA, SCA, POL/EUR, and EA/WR patterns as potential extratropical drivers. Likewise, the leading decadal-scale SST modes of midlatitude oceans, in particular the Pacific decadal oscillation (PDO) and the Atlantic multidecadal oscillation (AMO) are considered. To assess the tropical forcing of the WT composition, ENSO-related indices (Niño-1+2, Niño-3.4, Niño-4, SOI), the Indo-Pacific warm pool (WP) index, and the stratospheric QBO are incorporated. The Euro–Atlantic pressure modes (AO, NAO, EA, EA/WR, SCA, POL/EUR) as well as most of the SST indices (Niño-1+2, Niño-3.4, Niño-4, AMO, PDO) and tropical circulation modes (SOI, QBO) are available for download from the National Oceanic and Atmospheric Administration (www.esrl.noaa.gov/psd/data). The monthly mean SST of the Indo-Pacific WP (10°S–10°N, 120°–150°E) is extracted from the global ERSST, version 03, (v03) dataset (Smith and Reynolds 2003). The effect of teleconnections on the WT composition at a seasonal scale is assessed by means of a composite analysis, comparing the mean frequency of each weather type for seasons assigned to the first, second, and third tertile of the seasonal mean teleconnection index. Significant deviations (at the 10% significance level) from the overall mean WT frequency are derived by means of Students t test. To account for intraseasonal variations of the influence of large-scale climatic modes on the regional WT composition, spearman correlations between WT frequencies and teleconnection indices are computed at the monthly scale and significant correlations are highlighted. Correlations are only considered if the monthly mean relative WT frequency exceeds 10%.

c. *WTs and near-surface climate variables*

WTs are analyzed with regard to their spatial characteristics of temperature and precipitation anomalies, aiming at a detailed investigation of the influence of the interannual variability of the WT composition on the central Asian near-surface climate during boreal cold season. The 6-hourly fields of near-surface variables for the period 1979–2010 are obtained from the ERA-Interim/Land, which adjusts ERA-Interim modeling results with gridded GPCC observations at a monthly scale (Balsamo et al. 2015). Spatial fields of 6-hourly temperature anomalies are computed utilizing mean and standard deviation for each grid cell. Precipitation anomalies are computed in percent of the seasonal 6-hourly mean, that is, by dividing the deviation of the WT precipitation mean and the overall precipitation average by the overall mean, since precipitation values are highly skewed.

A WT-based reconstruction of temperature and precipitation fields is conducted to quantify the dependence of seasonal climate anomalies on interannual variations of the WT composition. The reconstruction is based on the assumption that the spatial distribution of 6-hourly temperature and precipitation values is constant for each WT over the entire period. Gridded seasonal temperature (precipitation) estimates are generated by multiplying the seasonal WT frequencies with the WT temperature mean (precipitation sum) for each grid cell. Seasonal temperature and precipitation reconstructions are cell-wise correlated with observations in order to assess the skill of the weather-type classification in reproducing the interannual variability and trends of near-surface climate variables. This makes it possible to quantify the independent influence of dynamic and thermodynamic variations and changes on the central Asian near-surface climate. In this context, dynamic variations and changes are defined as the portion of near-surface climate variability, which can be assigned to interannual anomalies of WT frequencies. Thermodynamic variations and changes represent WT internal anomalies of near-surface climate variables, which are not captured by the WT classification approach (Shepherd 2014; Murawski et al. 2018).

To depict the interannual variability of temperature and precipitation at a regional scale, areas with a with quasi-homogeneous seasonal climate variability are identified by means of a bootstrap-based clustering approach (Hennig 2007) applied to seasonal precipitation sums. A k-means clustering is applied to the time series of gridded precipitation anomalies and various artificial records, derived by means of bootstrap resampling, for a predefined range of cluster numbers ($k = 1$ to 10). The stability of the cluster solution is estimated for each number of k, based on the mean Jaccard coefficient, defined as the number of elements classified to the same cluster divided by the overall sample length. The best number of k corresponds to the minimum Jaccard coefficient. Time series of spatially averaged seasonal precipitation anomalies are analyzed and the influence of the seasonal WT composition is investigated for each subregion. We utilize the same regions for the investigation of the regional-scale temperature variability.

3. Results

a. *WTs and large-scale circulation patterns*

The CI record for $k = 2$ to 20 clusters and the CI confidence interval (Fig. 1) indicate a significantly improved classifiability for partitions into 2, 4, 5, and 8 clusters as well as for k values larger than 10. The

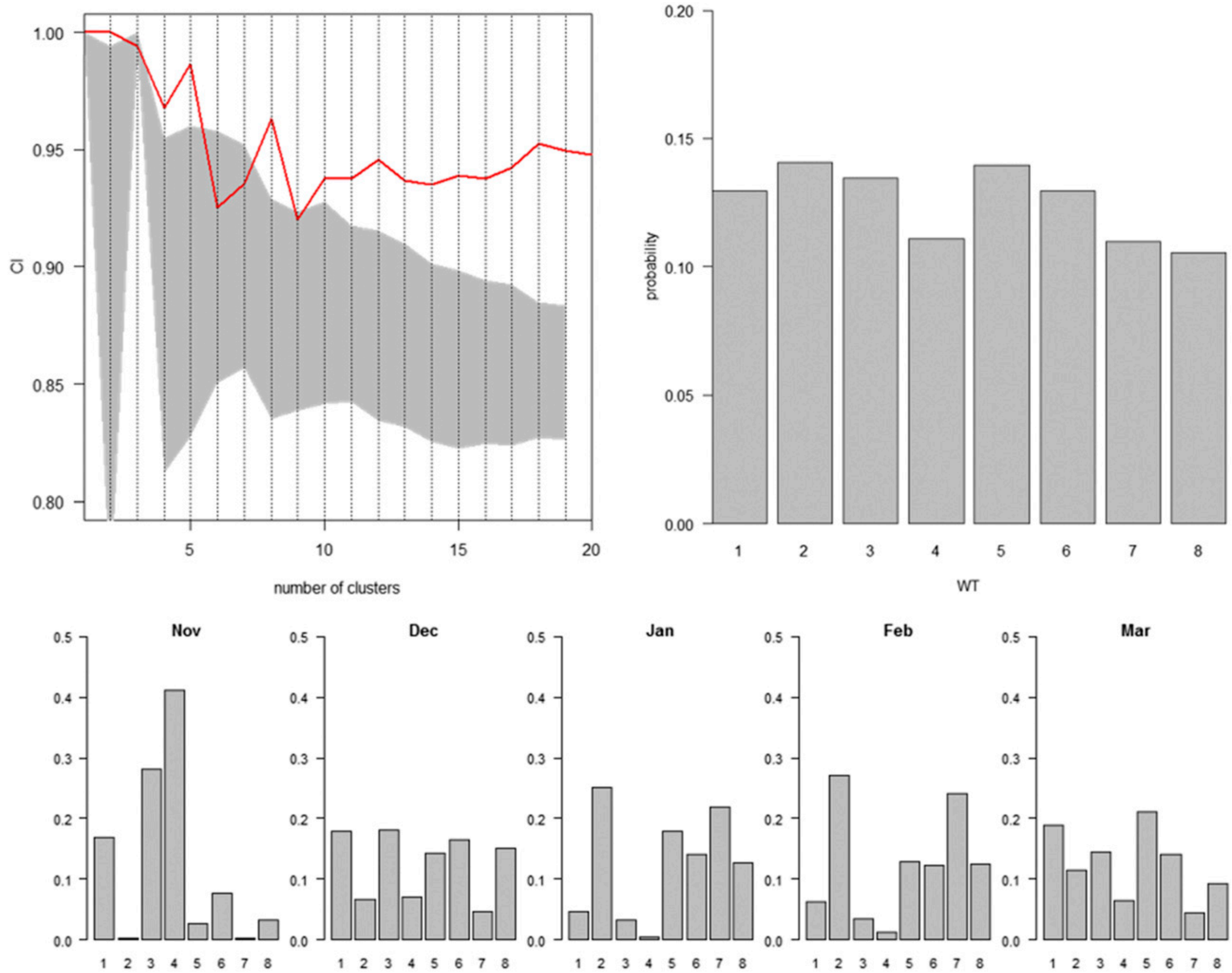

FIG. 1. (top left) The CI for k-means partitions with $k = 2$ to 20 clusters (red line) and the 90% confidence interval based on red-noise data (gray range). (top right) Relative frequency of WTs for the entire cold season (November–March) for the selected WT classification. (bottom) Relative frequencies of WTs for each month.

analysis of cluster solutions with 2, 4, and 5 clusters (not shown) reveals that those partitions mainly represent the seasonal cycle of GPH. The partition into 8 clusters identifies WTs representing both the seasonal cycle and intraseasonal variations of the regional circulation. Thus the analysis of cold season WTs for central Asia is performed based on the 8-cluster solution. All WTs have similar relative frequencies between 11% and 14% at the seasonal scale. At the monthly scale strong intraseasonal frequency variations are detected for some WTs (Fig. 1, lower panel). While WT1, WT3, and WT4 are typically observed during November and March, WT2, WT7, and WT8 mainly occur during the core winter season. On the contrary, WT5 and WT6 show almost constant relative frequencies.

The large-scale GPH patterns (Fig. 2) of WT1 and WT2 feature a strong anticyclonic anomaly over Russia and a cyclonic anomaly over Europe. Central Asia is the under influence of a Rossby ridge (R[CA] in Fig. 2) and the zone of maximum westerlies is distinctly shifted to the north. This results in divergent anomalies of vertically integrated moisture fluxes over central Asia (Fig. 3). WT1 is associated with positive GPH anomalies over the entire target region. WT2 features strong negative anomalies over northern India (C[Indic]), resulting in convergent anomalies of moisture fluxes (i.e., negative anomalies of moisture divergence) in the south of the target area.

WT3 shows an inverse GPH pattern, featuring a strong cyclonic anomaly over central Russia, while rather anticyclonic anomalies occur over Europe and southern and central Asia. A Rossby trough is distinctly defined over northern central Asia (R[KAZ]) and strong westerly moisture fluxes prevail over Kazakhstan

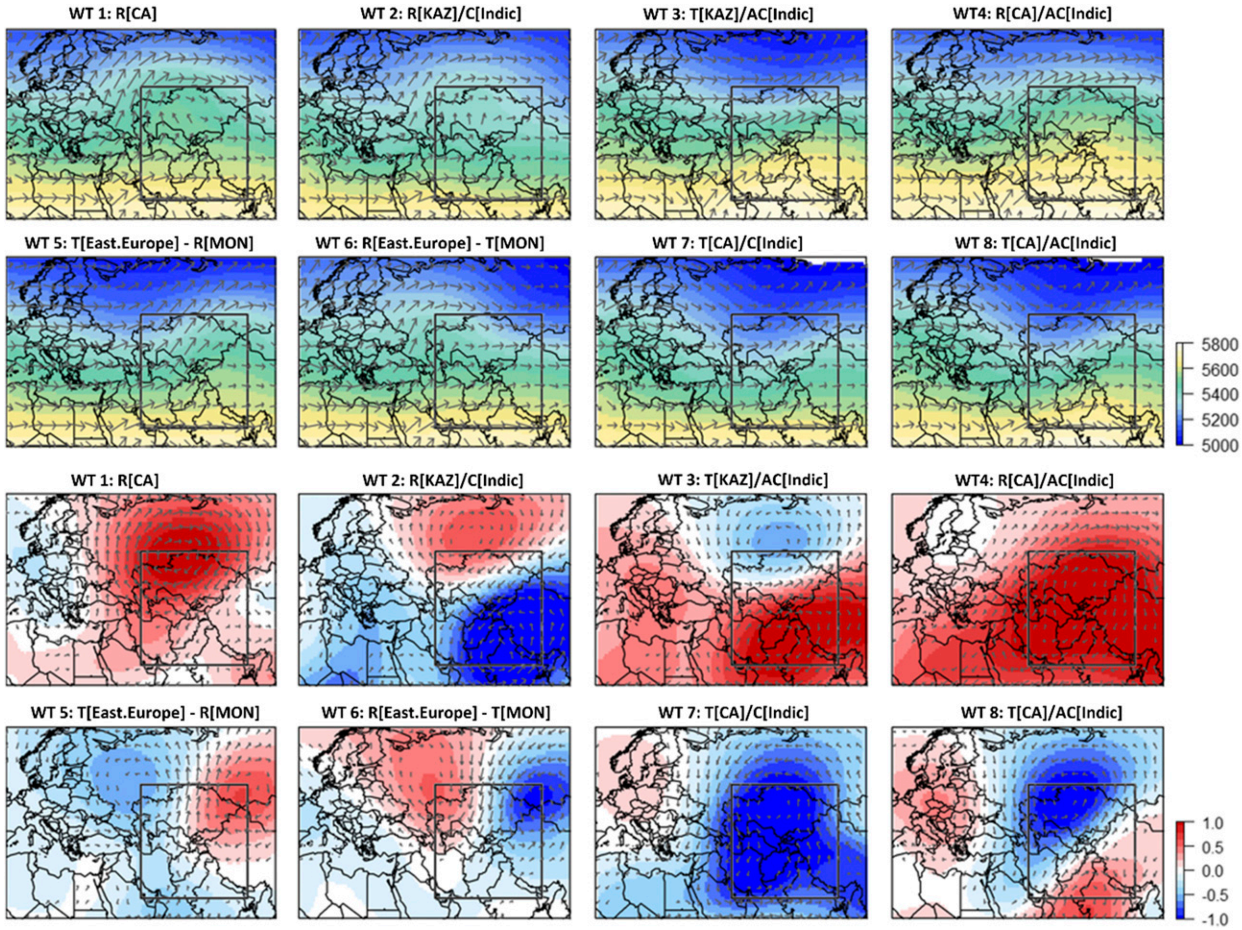

FIG. 2. (top rows) Composite maps of 6-hourly GPH (m) over Eurasia for each WT and associated vertically integrated moisture fluxes (arrows). (bottom rows) Corresponding anomalies of standardized GPH and moisture fluxes. Anomalies significant at $a = 0.1$ are shown. The box displays the region used for the WT classification approach. GPH anomalies in that region correspond to the centroids of the WT clusters. Acronyms indicate the major features (and their centers of action) for each WT: Rossby ridge (R), Rossby trough (T), anticyclonic anomaly (AC), cyclonic anomaly (C), central Asia ([CA]), Kazakhstan ([KAZ]), Mongolia ([MON]), and Indian Ocean and Indian subcontinent ([Indic]).

and the Tian Shan region. The entirety of central Asia is under the influence of southwesterly winds that intensifies the moisture advection from the Caspian Sea into northern central Asia. Convergent anomalies of vertically integrated moisture fluxes prevail in the north while divergent moisture fluxes are characteristic for the south of the target region. WT4 features positive GPH anomalies over the entirety of Eurasia, centering over central Asia. As for WT1 and WT2, the high pressure anomalies provoke a northward shift of the westerly jet stream. Because of the southward shift of the anticyclonic anomaly, compared to WT1 and WT2, a strong southerly flow is apparent over Turkmenistan, Uzbekistan, and western Kazakhstan. WT5 and WT 6 feature a dipole-like pattern of GPH anomalies between the northwest of the domain (including the Kazakh and the Russian plains west of the Ural Mountains) and the northeast (including the Tian Shan and the Altai mountain ranges). WT5 shows cyclonic circulation anomalies over northern and eastern Europe as well as southern Asia and anticyclonic anomalies over the Tian Shan and Altai mountains. The pattern is associated with the formation of a Rossby trough over the Caspian Sea and eastern Europe (T[East.Europe]) and a ridge over western China and Mongolia (R[MON]). It thus features an asymmetrical position of planetary wave tracks for central Asia. This results in strong southwesterly winds and an increased advection of moist and warm air masses from the Red Sea and Caspian Sea, particularly into the eastern part of the target domain. Only the Tian Shan region is characterized by divergent moisture fluxes (Fig. 3). The reverse pattern WT6 features a trough

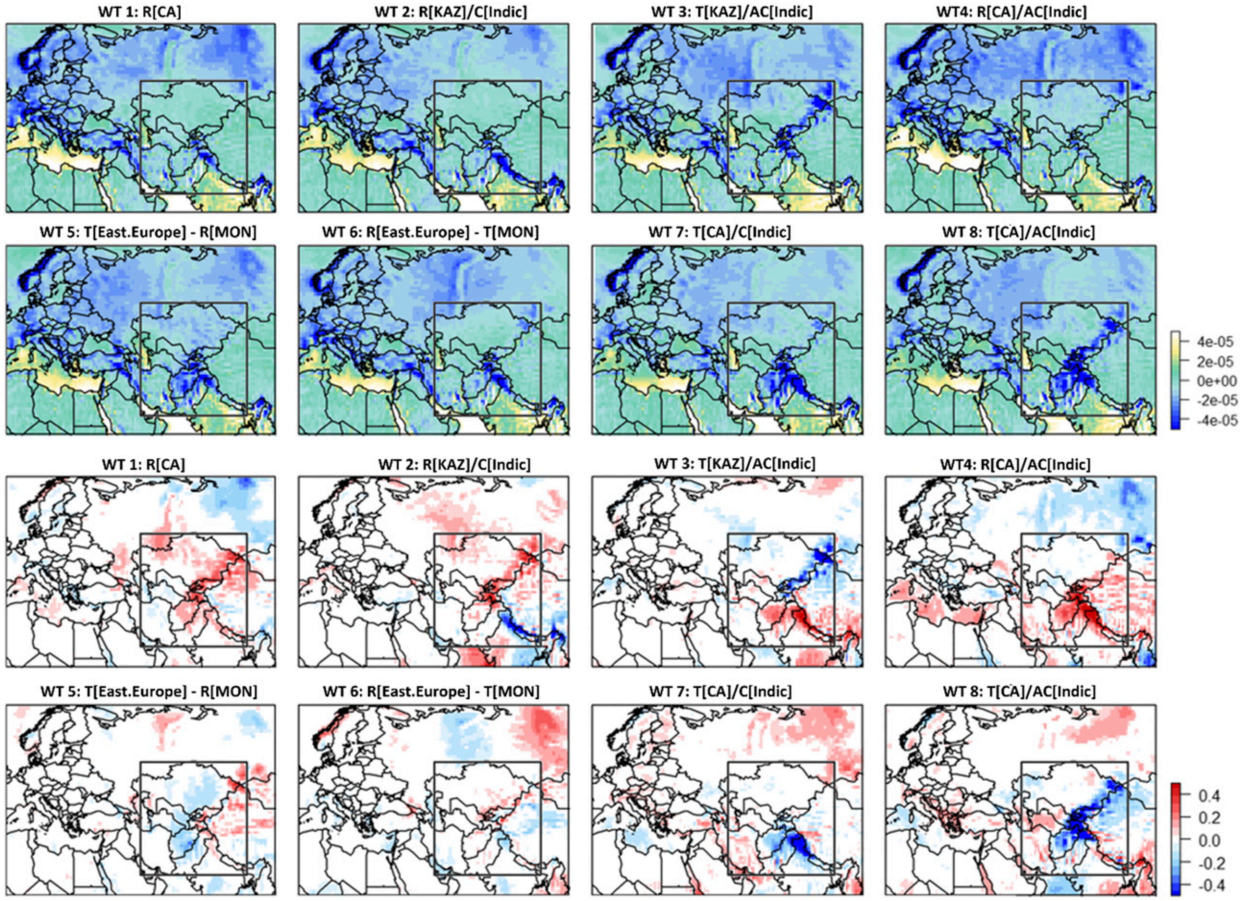

FIG. 3. (top rows) Composite maps of 6-hourly divergence of vertically integrated moisture fluxes [kg (m s)$^{-1}$] over Eurasia for each WT. Negative values indicate convergence, and positive values indicate divergence of moisture fluxes. (bottom rows) Corresponding anomalies of standardized vertically integrated moisture divergence. The box displays the region used for the WT classification approach.

situation over Mongolia and western China (T[MON]) and a ridge over western Kazakhstan and southwestern Russia (R[East.Europe]). The pattern is associated with northwesterly winds, particularly over Kazakhstan. Divergent anomalies of moisture fluxes prevail over central Asia with the Tian Shan and Pamirs regions being an exception. WT7 and WT8 characterize typical winter patterns and feature a strong cyclonic anomaly over central Asia and Russia and anticyclonic anomalies over Europe. A Rossby trough is located over Kazakhstan and Uzbekistan (T[CA]) and the frontal jet stream is shifted toward south. Compared to WT3, the Rossby trough is distinctly more pronounced and the entirety of central Asia is under influence of strong westerlies. Southwesterly moisture fluxes prevail over the target region, advecting moisture from the Red Sea and the Arabian Gulf. Compared to WT7, which features strong negative GPH anomalies over the entire target region, the center of the cyclonic anomaly in WT8 is shifted northward and high pressure anomalies prevail over southern Asia and the Indian Ocean (AC[Indic]). The consequential anticyclonic anomaly intensifies the southwesterly flow over Iran and Afghanistan and increases the tropical supply of moisture and heat from the Red Sea and the Arabian Gulf. WT7 is characterized by convergent anomalies of moisture fluxes over the Pamirs and the Karakoram Range. The Tian Shan is located leeward of the southwesterly flow, resulting in locally divergent anomalies. WT8 features convergent anomalies of moisture fluxes for the entirety of central Asia (Fig. 3).

The results suggest that WTs prevailing over central Asia are embedded in large-scale atmospheric patterns and might be interpreted as regional manifestations and superpositions of tropical and extratropical circulation modes propagating into the target region from the Euro–Atlantic domain and the Indian Ocean, respectively. The weather-type classification clearly identifies the southward shift of the polar frontal zone during January and February, which is associated with negative pressure anomalies over the entire target region. The

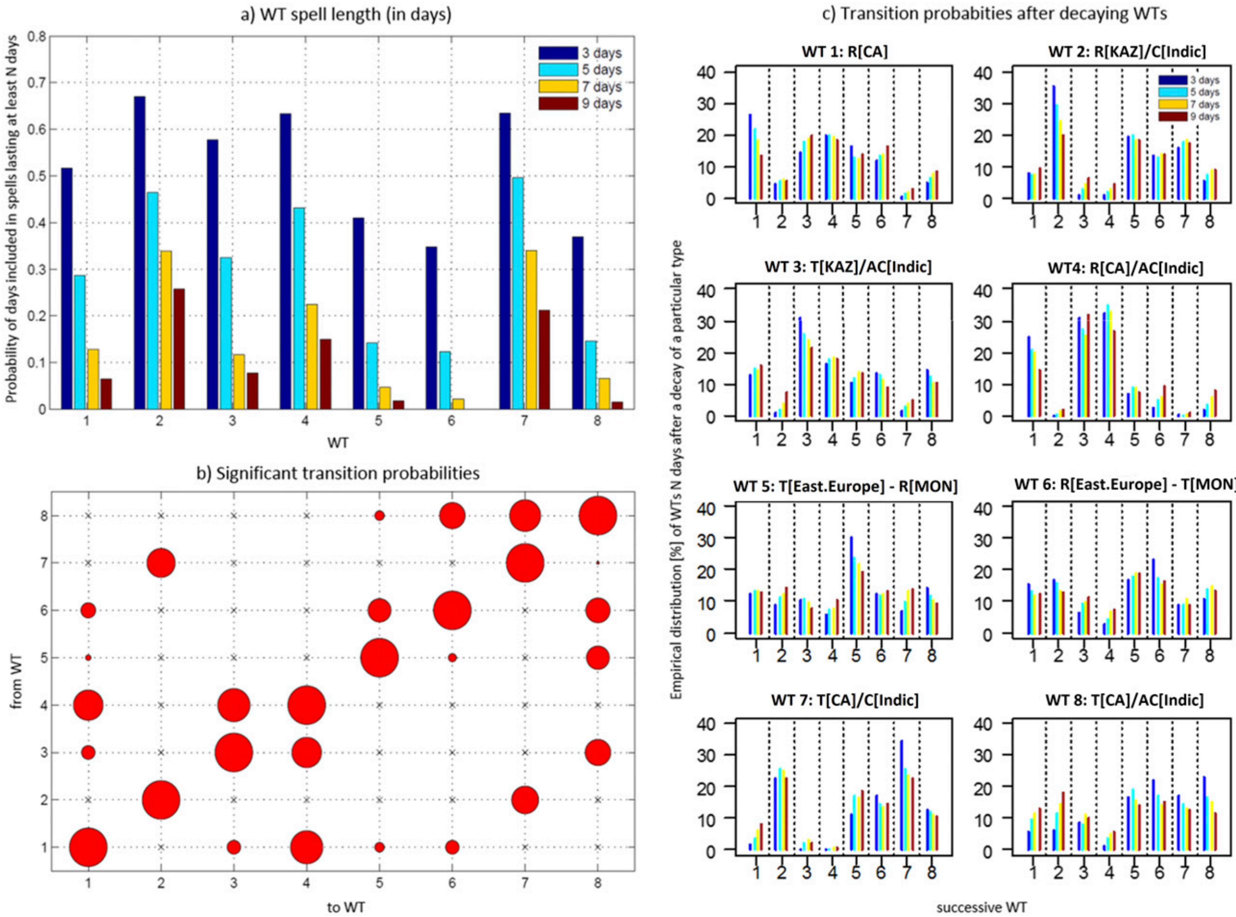

FIG. 4. WT spell lengths and transitions. (a) Proportion of WT days included in spells of consecutive WTs lasting at least 3, 5, 7, and 9 full days. (b) Significant probability transitions from one WT to another one. The probability transitions are computed and tested for significance for 28 lags, i.e., from one step to 6 h later to from one step to 7 days later. The size of the red circle is proportional to the number of significant transitions ($p = 0.01$) vs 1000 random reshufflings of the WT time series, cross indicates that transitions never reach $a = 0.01$ for any lag. (c) Empirical distribution (%) of successive WTs 3, 5, 7, and 9 days after a decay of a particular type.

winter patterns (particularly WT2 and WT7) are all characterized by strong negative GPH anomalies over the southern target domain. The regional manifestation of pressure cells alters the atmospheric circulation over central Asia and accounts for intraseasonal variations of moisture fluxes. Enhanced westerlies are linked to the formation of a Rossby trough that centers over Kazakhstan and is bordered by the central Asian mountain ranges (WT3, WT7, and WT8). WTs associated with a Rossby ridge over central Asia are characterized by a weakened westerly flow and rather divergent flow conditions (WT1, WT2, and WT4). The manifestation of asymmetrical planetary wave tracks (WT5 and WT6) leads to regionally varying circulation conditions. GPH variations over South Asia and the Indian Ocean regulate the tropical moisture supply. The formation of a high pressure cell over northern India (WT8) leads to enhanced southwesterly winds at its northwestern edge and advects warm and moist air masses into the target domain. On the contrary, WTs featuring negative pressure anomalies and a cyclonic circulation over India (WT2 and WT7) are characterized by an attenuated southwesterly flow.

b. WT spell lengths and transitions

The analysis of spell lengths (Fig. 4a) shows strongest persistence of WT2 and WT7, with more than 60% of spells lasting longer than three days and roughly 20% of spells lasting longer than nine days. The fact that these WTs are characterized by strong negative GPH anomalies over southern Asia and the Indian Ocean indicates a rather persistent behavior of the tropical influence on the central Asian climate, while the Northern Hemispheric circulation modes are characterized by a high frequent variability. Besides self-transitions, indicating a short- to midterm persistence for all WTs, statistically significant transitions (Fig. 4b) of WT2 are only detected with WT7 and vice versa, indicating that those patterns form a group of jointly appearing circulation characteristics. The relative distribution of WTs after the decay of WT7 (Fig. 4c) shows a transition to WT2 after 3, 5, 7, and 9 days in more than 25% of cases, which is only exceeded by a recovery of WT7 (self-transition). In 10%–15% of cases a succession of WT7 to WT5 and WT6 is detected, demonstrating that those patterns represent a transition state between the WT2–WT7 group and all other WTs. Frequent transitions (between 15% and 30%) are detected for a group including WT1, WT3, and WT4, which mainly occurs during November, December, and March. Those WTs feature rather positive GPH anomalies over southern Asia and differ in their Eurasian pressure patterns and the associated Northern Hemispheric wave tracks. These transitions indicate an eastward propagation of Rossby waves and a characteristic sequence of trough and ridge conditions, which modifies the strength and location of the westerly jet stream over central Asia. Particularly WT5, WT6, and WT8 rarely occur longer than 7 days (below 5% of all spells) and WT5 and WT6 show almost constant transitions with all WTs. Taking into consideration the brevity of WT5 and WT6 spells this indicates that these asymmetrical patterns depict a transient circulation state, while the manifestation of a Rossby ridge (WT2 and WT4) or trough (WT3 and WT7) centered over central Asia represents rather stationary conditions.

c. *WT frequencies and tropical and extratropical teleconnections*

Central Asian weather types resemble typical large-scale planetary wave tracks and are closely related to Euro–Atlantic circulation modes. Those patterns featuring an anticyclonic anomaly over Russia and central Asia (R[CA], R[KAZ]) and a cyclonic anomaly over Europe (WT1, WT2, and WT4) resemble the negative manifestation of the EA/WR pattern (see e.g., Krichak and Alpert 2005). At the seasonal scale, the frequency of WT1 is significantly reduced during the positive phase of AO (−15.8%, Fig. 5) and POL/EUR (−17.2%). However, important relationships might be blurred because of the seasonal averaging of both WT frequencies and climate indices. Monthly correlations between the WT1, WT2, and WT4 frequencies and the EA/WR index are strongly negative (up to −0.65) and partially significant (Fig. 6). WT1 and WT2 show positive correlations with the SCA pattern, while negative correlations are apparent for WT4. Correlations with AO/NAO are marginal for WT1 and WT4 frequencies, while WT2 is more likely during the positive phase of NAO/AO. On the contrary, WT3, WT7, and WT8, all featuring a Rossby trough over central Asia (T[CA], T[KAZ]) and an associated southward shift of the westerly jet stream, show strongly positive and mostly significant correlations with the EA/WR pattern at the monthly scale (Fig. 6). Consistently, positive anomalies of WT frequencies at the seasonal scale are observed during the positive state of the EA/WR index for WT7 and WT8 (Fig. 5). Further, for all WTs characterized by a planetary trough over central Asia, positive correlations with NAO/AO are apparent at the monthly scale. Mainly negative frequency anomalies during the negative AO state (up to −24.7% for WT3) are detected at the seasonal scale. WT3 shows a significantly decreased frequency during the positive state of POL/EUR (−25.2%). The asymmetrical patterns WT5 and WT6 clearly resemble the negative and positive states of the Scandinavian pattern, respectively (Bueh and Nakamura 2007). As expected, a strong negative (positive) correlation between monthly WT frequencies and the SCA index is observed for WT5 (WT6). Both WT5 and WT6 are characterized by a strong meridional flow and are more likely during the negative state of AO (+18.7%, +18.1%; Fig. 5).

Besides Northern Hemispheric wave tracks, WTs and their frequencies are influenced by tropical teleconnections, particularly by ENSO. Monthly frequencies of WTs featuring a Rossby ridge over central Asia (WT1, WT2, WT4; R[CA], R[KAZ]) are mostly negatively (although not significantly) correlated with SST anomalies in the central Pacific (Niño-1+2, Niño-3.4, Niño-4), indicating a stimulation of anticyclonic circulation anomalies over central Asia during La Niña events. Further GPH anomalies over southern Asia appear to be strongly linked to interannual variations of ENSO, which is depicted by mainly negative correlations of WT frequencies with ENSO-related indices for WT2 and WT7 (C[Indic]) and rather positive correlations for WT8 (AC[Indic]). Frequencies of WT7 and WT8, which feature similar GPH patterns over Eurasia, but a strongly different behavior over the Indian Ocean, reveal fundamental differences in their statistical relationships with ENSO-related indices (negative correlations up to $r = -0.4$ for WT7 and positive correlations up to $r = 0.45$ for WT8). At the seasonal scale a significant frequency increase of WT8 is depicted for negative SST anomalies over the Indo-Pacific WP as well as for positive anomalies of the Niño-3.4 index.

The correlation of seasonal mean 500-hPa GPH over the northern Indian Ocean (not shown) amounts to values up to +0.4 indicating that positive pressure anomalies over the south of the target domain are triggered by El Niño conditions because of its impact on the Walker circulation and the strength of the regional Hadley cell (Mariotti 2007). The resulting anticyclonic

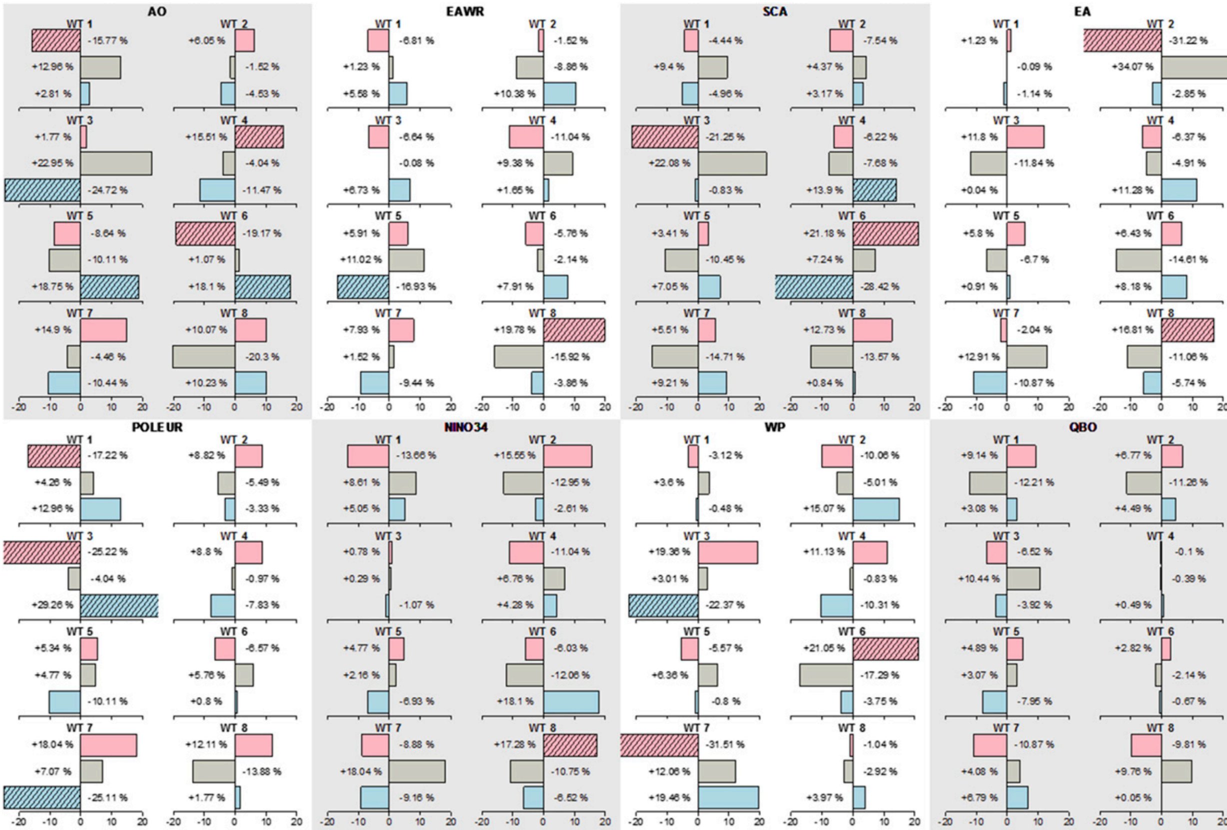

FIG. 5. Influence of seasonal mean teleconnection indices on the seasonal frequency of WTs. Data are divided into seasons representing a rather negative (0%–33% quantile, blue bars), normal (33%–66% quantile, gray bars), and positive state (66%–100% quantile, red bars) of the considered index, and the mean seasonal WT frequency anomaly (%) is depicted. Statistically significant deviations (t test, $a = 0.1$) from the overall frequency mean are marked (striped).

circulation over southern Asia leads to an enhanced southwesterly flow and intensified moisture supply from the tropical oceans into the target domain. Under La Niña conditions tropical moisture fluxes into central Asia are reduced.

Summarizing, results indicate that the EA/WR pattern has the strongest influence on the regional circulation over central Asia, with enhanced westerly winds prevailing during its positive phase. NAO/AO controls the westerly circulation and the stationary manifestation of a Rossby trough over central Asia is more likely during its positive state (WT3, WT7, and WT8). SCA leads to a regional modification of circulation anomalies with weakened (intensified) westerlies over the northwest (northeast) of the target domain during its positive phase (WT5) and vice versa during its negative phase (WT6).

Tropical drivers, in particular ENSO, further modify the regional circulation because of the provocation of an anticyclonic anomaly over the Indian Ocean during the ENSO warm phase, which intensifies southwesterly moisture fluxes into central Asia. A slightly increased frequency (though not significant) of WTs featuring an anticyclonic anomaly over central Asia is detected, indicating an indirect teleconnection between tropical circulation modes and westerly wave tracks, as proposed by Barlow et al. (2002).

d. *WT and near-surface climate variability*

The spatial distribution of seasonal (November–March) mean temperatures over central Asia (Fig. 7b) follows the latitudinal gradient with temperatures below −5°C in northern Kazakhstan and positive temperatures prevailing in southern Uzbekistan, Turkmenistan, and Afghanistan. The complex topography (Fig. 7a) results in a pronounced spatial variability of surface climates at the regional scale. High mountain regions such as Tian Shan, Pamirs, and Hindu Kush are characterized by mainly negative temperatures. Precipitation is associated with the uplift of the westerly flow and seasonal precipitation sums exceed 500 mm at west-facing slopes of Tian Shan, Pamirs, and Karakoram

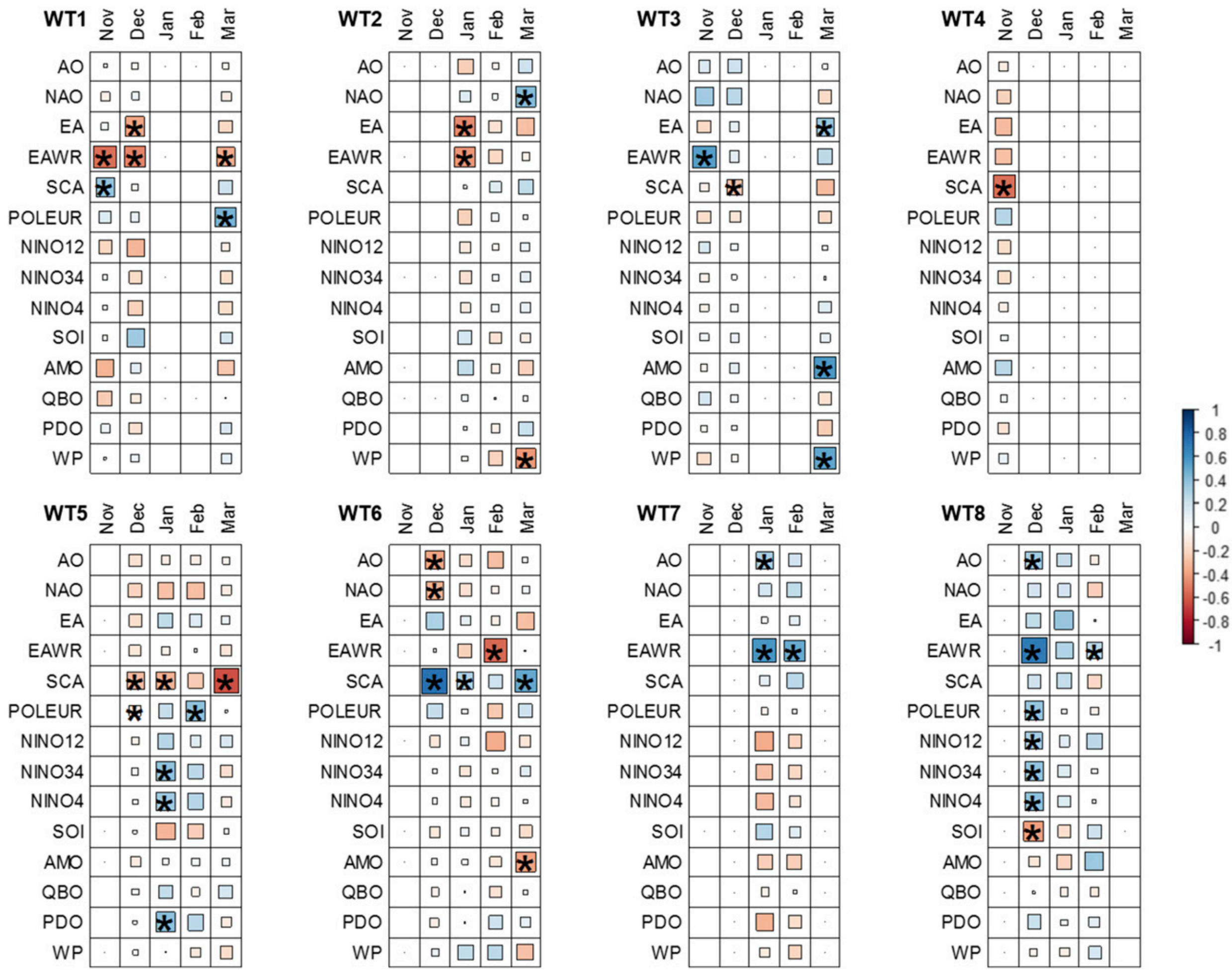

FIG. 6. Spearman rank correlation coefficient between the monthly state of selected teleconnection indices and the corresponding frequencies of WTs. Significant correlations are marked (*, $a = 0.1$). Correlations are only depicted if the monthly mean relative WT frequency exceeds 10%.

Range (Fig. 7c). Lower mountain ranges such as the Kazakh uplands and Hindu Kush typically receive seasonal precipitation sums in the order of 250–350 mm, while arid conditions are characteristic for the vast central Asian plains (<200 mm). Three clusters of homogenous cold season climate variability (Fig. 7d) are found by means of the bootstrap-based clustering approach of seasonal precipitation anomalies. Subregion 1 covers the northern Kazakh plains and is bordered by the Kazakh uplands. Subregion 2 encompasses southern Kazakhstan, Uzbekistan, Kyrgyzstan, Tajikistan, and northern Turkmenistan and extends to the mountain barriers of Pamirs and Elburz. Subregion 3 includes the territories of Iran, Afghanistan, and Pakistan. In the following section, these regions are utilized to assess the influence of the seasonal WT composition on interannual variations of temperature and precipitation at the regional scale.

1) TEMPERATURE

Temperature anomalies for each WT (Fig. 8) in general reflect the seasonal cycle of WT frequencies, with mainly positive temperature anomalies in the entire target domain for WT1, WT3, and WT4 (main occurrence in November and March) and negative anomalies for WT2, WT7, and WT8 (representing typical winter patterns). Regional modifications of temperature anomalies are linked to prevailing wind directions. Strongly negative temperature anomalies are caused by northerly anomalies of the wind field and an associated advection of polar air masses. Positive anomalies usually coincide with southerly flow directions. Thus, the position of planetary waves over Eurasia controls the spatial distribution of temperature anomalies over central Asia. The formation of a Rossby trough (WT3, WT7, and WT8; T[KAZ], T[CA]) is accompanied by cold air advection

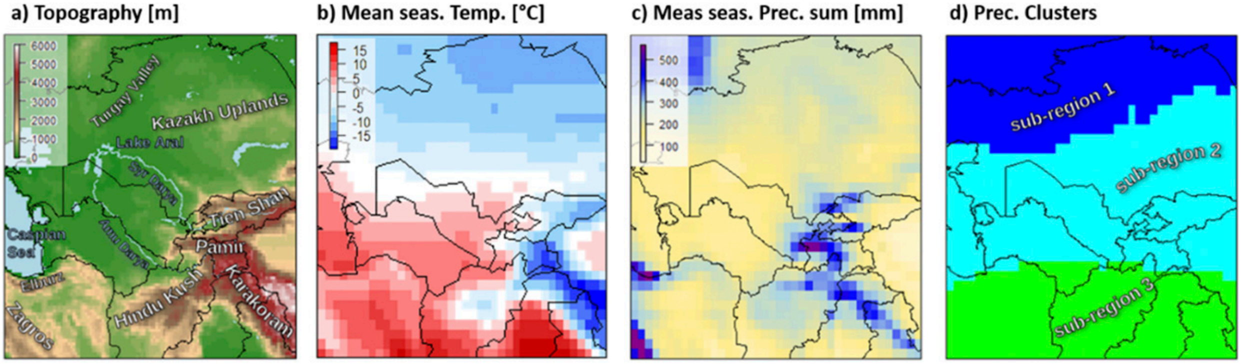

FIG. 7. (a) Topography of the central Asian region. (b),(c) Spatial distribution of mean seasonal temperature and seasonal precipitation sums (November–March, based on ERA-Interim/Land) for the period 1979–2010. (d) Homogeneous regions of precipitation variability, based on cluster analysis of gridded seasonal precipitation.

at its western flank, resulting in rather negative temperature anomalies over western Kazakhstan, Uzbekistan, and Turkmenistan, while anomalous high temperatures prevail over the east of the target region. A Rossby ridge centered over central Asia (WT1, WT2, and WT4; R[CA], R[KAZ]) leads to a reversed distribution of temperature anomalies. Minimum temperatures over eastern Kazakhstan and the Tian Shan in WT2 coincide with a northerly flow at the eastern flank of a planetary wave. The asymmetrical WT5 and WT6 are characterized by a strong meridional flow resulting in positive and negative temperature anomalies in northern central Asia, respectively. Pressure anomalies over the Indian Ocean modulate the southwesterly flow into central Asia and affect temperature anomalies along an axis incorporating the Hindu Kush, Pamirs, and Tian Shan mountain ranges. An intensified southwesterly current (WT8; AC[Indic]) advects tropical air masses and is

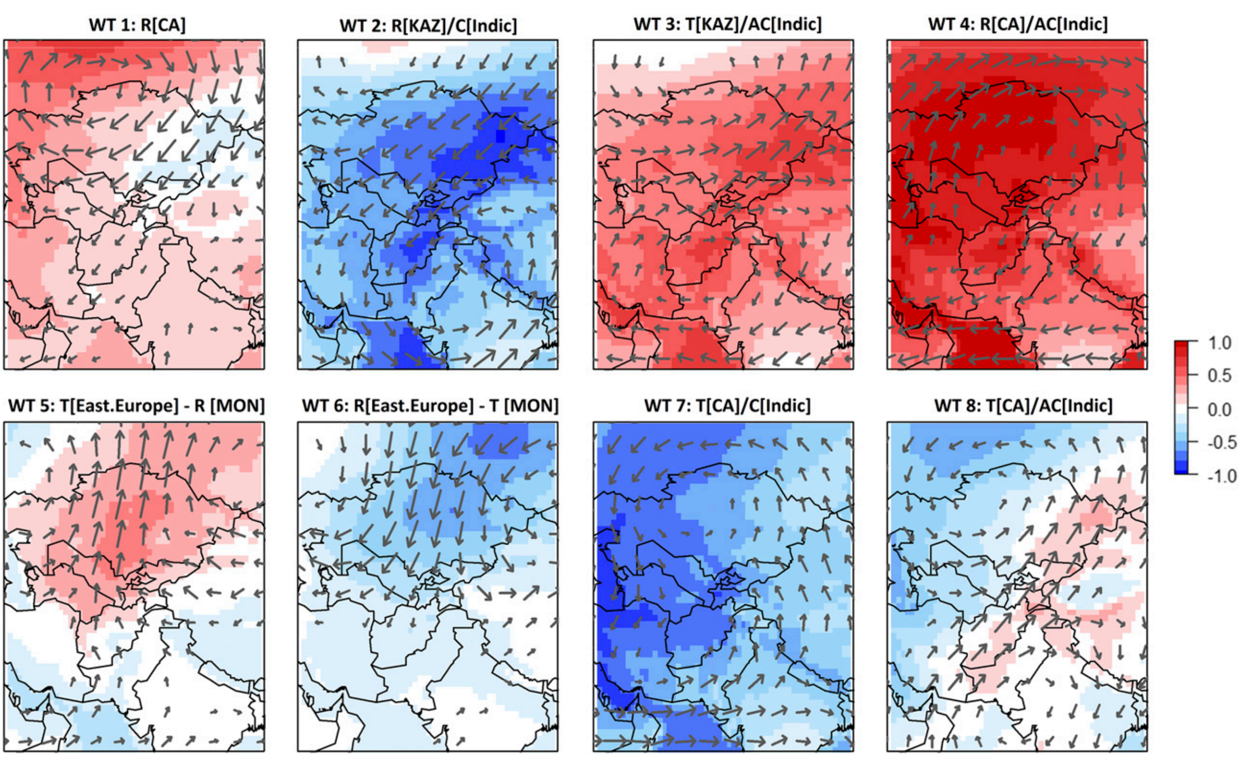

FIG. 8. Composite maps illustrating the averaged anomalies of ERA-Interim/Land 6-hourly temperature for each weather type. Values are depicted in standard deviations for each grid cell, respectively. Arrows indicate anomalies of the 500-hPa ERA-Interim wind field.

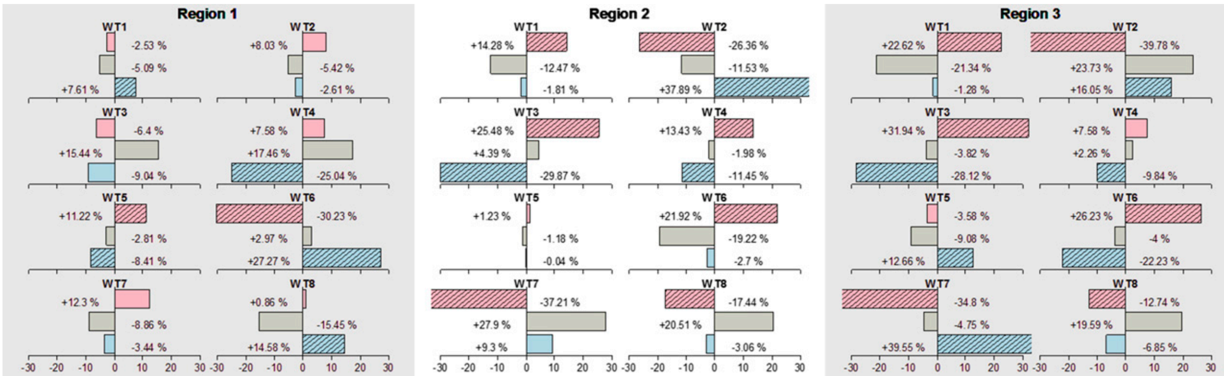

FIG. 9. Anomalies of seasonal WT frequencies (in % of the frequency mean) during years featuring cold (0%–33% quantile of mean temperatures, blue bars), normal (33%–66% quantile, gray bars), and warm (66%–100% quantile, red bars) conditions in the central Asian subregions. Statistically significant deviations from the overall frequency ($a = 0.1$) mean are striped.

accompanied by positive temperature anomalies. On the contrary, a weakened tropical contribution because of cyclonic anomalies over the Indian Ocean (WT2 and WT7; C[Indic]) causes strongly negative temperatures.

The analysis of WT frequencies during cold and warm years (defined as the lower and upper tertile for each cluster region; Fig. 9), demonstrates that variations of seasonal mean temperatures are linked to anomalies of the WT compositions. Cold winters in subregion 1 (northern Kazakhstan) are observed during years with decreased frequencies of WT4 and WT5 and increased frequencies of WT6. For subregion 2 and subregion 3 cold winters show an increased frequency of the cold WTs (WT2 and WT7) and a decreased occurrence of the rather warm WTs (WT3, WT4, WT5).

Correlations between observed and WT-based reconstructed seasonal mean temperatures (Fig. 10) are positive for the entire domain and exceed values of 0.9 over Kyrgyzstan, Tajikistan, and Afghanistan. Spatially averaged correlations amount to 0.37, 0.79, and 0.88 for subregions 1, 2, and 3. This indicates that seasonal temperature anomalies are strongly controlled by dynamical variations of the regional circulation, particularly for subregions 2 and 3. Time series of observed and reconstructed temperature anomalies show that the WT classification captures exceptionally cold and warm years for subregions 2 and 3. The time series of the WT compositions (Fig. 10, lower panel) illustrates that warm winters in region 2 and region 3 (e.g., 1981, 1988, 1999, 2002, 2004, 2009, and 2010) are triggered by a reduced frequency of the typical winter patterns WT2, WT7, and WT8 and (for some years) an increased frequency of WT3. Cold winters (1983, 1984, 1997, 1998) show a reversal WT composition, giving evidence that reduced seasonal temperatures are associated with the frequent or persistent formation of a strong Rossby trough (WT7 and WT8; T[CA]) over central Asia.

Observed seasonal temperature trends for the period 1979–2010 over central Asia amount to 0.05°–0.1°C yr^{-1} with highest values over Kazakhstan and the Tian Shan region and slightly negative values over the northernmost target domain. Spatially averaged temperature trends amount to 0.06°C yr^{-1} for subregions 2 and 3. The spatial distribution of trends is reproduced by the reconstructed time series, however, with a reduced magnitude of 0.02°–0.04°C yr^{-1} (0.03°C yr^{-1} for subregions 2 and 3). This illustrates that roughly 50% of seasonal warming can be assigned to dynamical changes of the regional circulation. Statistically significant negative trends of WT frequencies are detected for the cold patterns WT2 and WT7 that account for an increased incidence of warm winter seasons after 1995.

2) PRECIPITATION

Anomalies of 6-hourly precipitation sums for each WT (Fig. 11) indicate that rainfall generation is associated with westerly anomalies of the wind field and an intensification of westerly moisture fluxes. Particularly the southward shift of the frontal jet stream as a consequence of the formation of a Rossby trough over central Asia (WT3, WT7, and WT8; T[KAZ], T[CA]) results in strongly positive precipitation anomalies with maximum values at the windward slopes of the mountain barriers. The zone of maximum precipitation is strongly linked to the magnitude of the planetary wave. While the formation of a Rossby trough over Kazakhstan (WT3; T[KAZ]) results in a dipole of positive and negative precipitation anomalies over the north and the south of the target region, a more pronounced shape of the planetary wave leads to increased westerly moisture fluxes and positive precipitation anomalies over all of central Asia (WT7 and WT8; T[CA]). On the contrary, anticyclonic anomalies associated with the formation

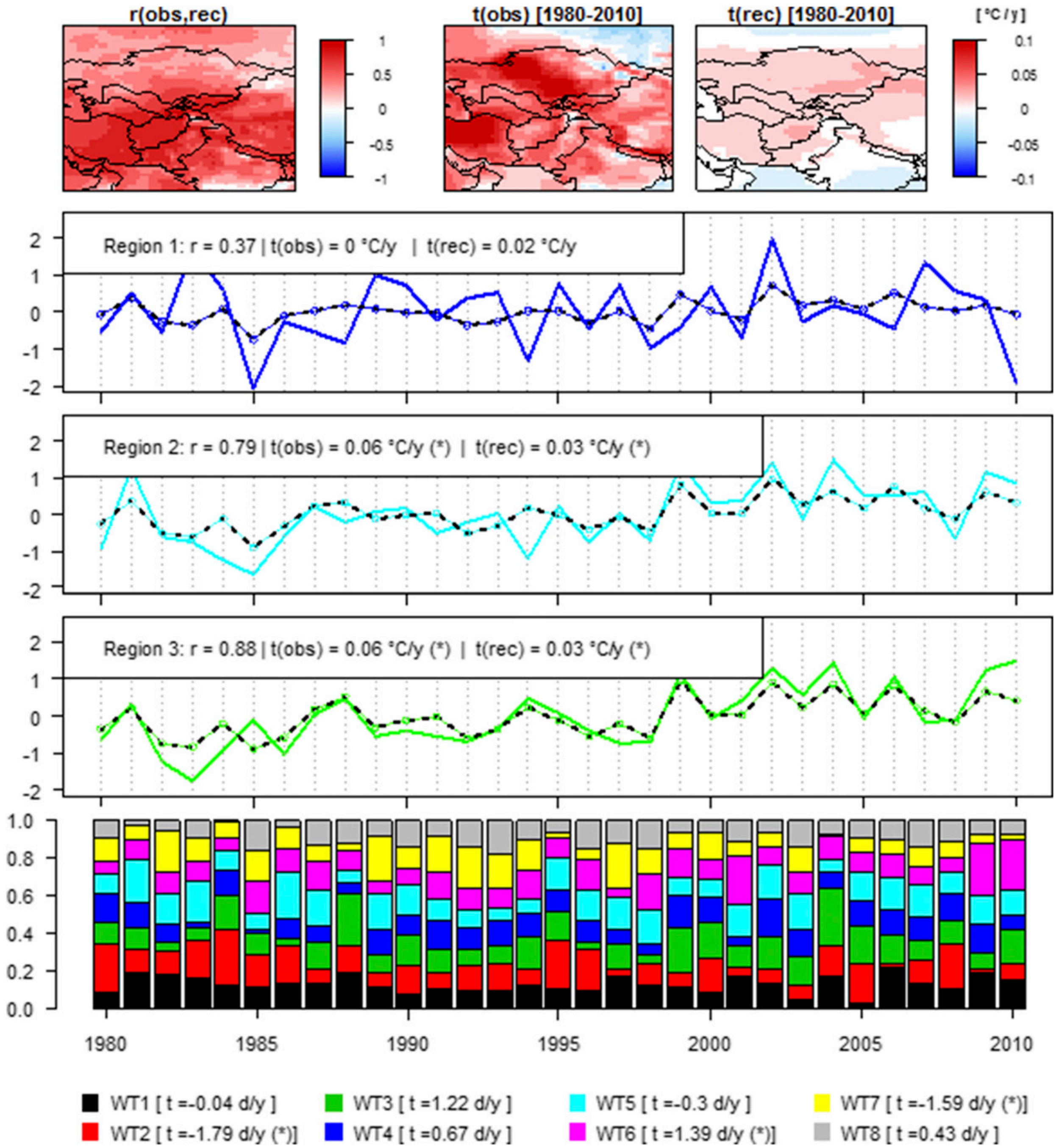

FIG. 10. (top) Spatial field of correlations between observed and WT-reconstructed seasonal mean temperatures [r(obs,rec)], trends of observed [t(obs)], and reconstructed [t(rec)] temperatures for the extended winter seasons from 1979 to 2010. (middle) Line charts show the time series of observed and reconstructed temperature anomalies (in std dev of observations) for each subregion. Correlations between spatially averaged observations and reconstructions are depicted as well as observed and reconstructed temperature trends. (bottom) The bar chart illustrates the time series of relative WT frequencies. Trends of seasonal WT frequencies (days yr^{-1}) are depicted and statistically significant trends are highlighted (*).

of a Rossby ridge over central Asia (WT1, WT2, and WT4; R[KAZ], R[CA]) result in a northward shift of westerly moisture fluxes and negative precipitation anomalies. In general, regions with positive (negative) precipitation anomalies are consistent with convergent (divergent) anomalies of vertically integrated moisture fluxes (Fig. 3). Besides zonal anomalies of the wind field, anomalous meridional moisture fluxes control the

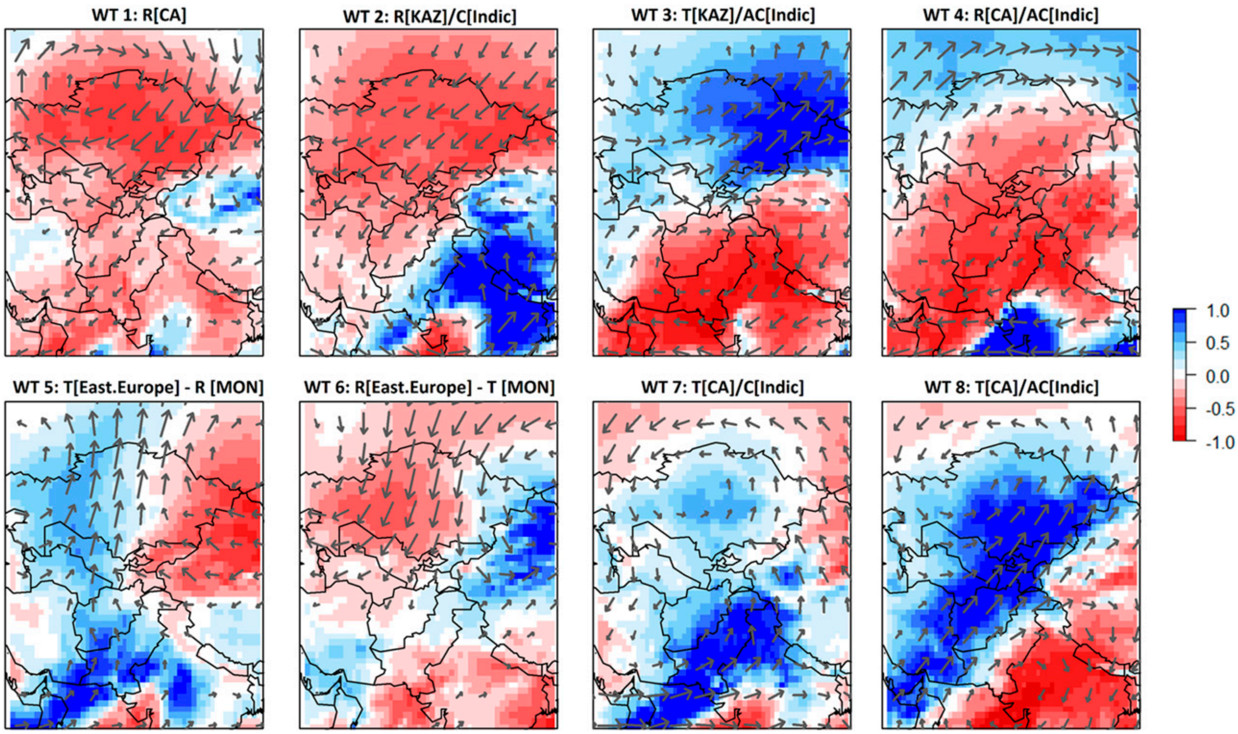

FIG. 11. Composite maps illustrating the averaged anomalies of ERA-Interim/Land 6-hourly precipitation sums for each weather type. Values are depicted relative to the seasonal mean 6-hourly precipitation sum [% $(100)^{-1}$] for each grid cell, respectively. Arrows indicate anomalies of vertically integrated moisture fluxes.

spatiotemporal precipitation variability over central Asia. WT5, associated with southwesterly winds over central Asia, is characterized by an increased advection of moisture from the Arabian Gulf, Red Sea, and Caspian Sea, particularly into the western part of the target domain. Only the Tian Shan region is characterized by a divergent flow and negative precipitation anomalies because of weakened westerlies. The reversal pattern WT6 features northwesterly winds over most of central Asia and is associated with divergent anomalies of moisture fluxes and dry conditions, with the Tian Shan and Pamirs regions being an exception.

As for shown for temperature, pressure anomalies over the Indian Ocean modulate the southwesterly flow over central Asia and the advection of moist tropical air masses from the Red Sea and the Arabian Gulf. Intensified southwesterly winds lead to moist conditions in the entire domain (WT8; CA[Indic]). WT7, which features a similar circulation over northern Eurasia but cyclonic anomalies over southern Asia (C[Indic]), is characterized by reduced precipitation amounts because of a weakened tropical moisture supply. Further, the Tian Shan is located leeward of the southwesterly flow in WT7, resulting in rather dry conditions, which demonstrates the role of the relative position of major orographic barriers to the prevailing flow direction.

The analysis of the interannual variability of seasonal WT frequencies shows that dry and moist conditions during the cold season in the subregions of central Asia are related to the occurrence of particular WTs (Fig. 12), although results are less significant compared with the analysis of temperature variations. An enhanced frequency of WT1 is associated with rather dry conditions in the entire target region at the seasonal scale. Deviations between the mean WT frequency during dry and moist conditions are statistically significant for subregions 1 and 3. Likewise a high frequency of WT2 corresponds to rather dry conditions in subregions 1 and 2. The strong meridional gradient of the WT3 precipitation distribution leads to significant positive precipitation anomalies in the Tian Shan region (subregion 2) and negative anomalies in the south of central Asia (subregion 3). WT4 shows an increased frequency during dry conditions in subregions 1 and 2 only, although the pattern is associated with negative precipitation anomalies in the entire target region. For WT5, a statistically significant frequency increase during moist conditions is detected for subregion 1 and subregion 3. WT7 is significantly more frequent during moist seasons

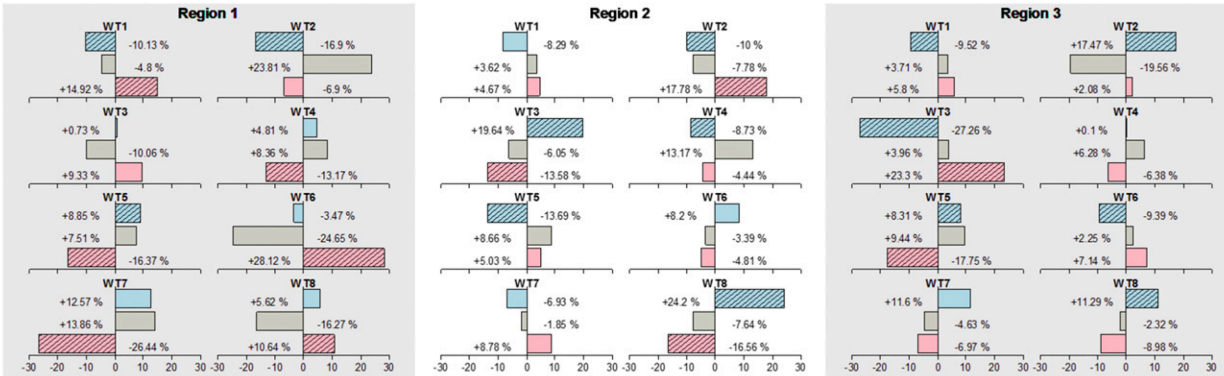

FIG. 12. Anomalies of seasonal WT frequencies (in % of the frequency mean) during years featuring dry (0%–33% quantile of seasonal precipitation sum, red bars), normal (33%–66% quantile, gray bars), and moist (66%–100% quantile, blue bars) conditions in the central Asian subregions. Statistically significant deviations from the overall frequency mean ($a = 0.1$) are striped.

in subregions 1 and 3. The fact that no clear relationship between seasonal precipitation anomalies and the frequency of WT7 is found for subregion 2, although the pattern is obviously associated with positive precipitation anomalies, might point to the limitations of the univariate approach. On the contrary, the frequency of WT8 is enhanced during moist conditions in all central Asia subregions, though significant results are only obtained for subregions 2 and 3.

The time series of observed and reconstructed seasonal precipitation anomalies for central Asian subregions (Fig. 13) indicate that interannual variations are only partially explained by anomalies of the WT composition. Correlations between observations and reconstructions amount to $r = 0.32$, $r = 0.38$, and $r = 0.35$ for subregions 1, 2, and 3, respectively. Reconstructed precipitation amounts show a strongly reduced variance, indicating a large WT internal precipitation variability. The spatial distribution of correlations between observed and reconstructed precipitation amounts exhibits a strong variability with maximum correlations up to $r = 0.7$ in the high mountain regions of Tian Shan and Altai, implying that orographic-induced precipitation is strongly linked to the prevailing flow direction, while precipitation anomalies over the dry central Asian plains are less predictable.

Major structures of the precipitation time series are captured by the WT-based reconstructions. This is particularly obvious for the rather moist period during the early 1990s and the frequent occurrence of dry conditions after 1999 in subregion 3. Particularly WT2 features a strong interannual variability with relative frequencies ranging from 4% to 29.5%. Seasons with a frequent occurrence of WT2 (e.g., 1984, 1995, 1996, and 2008) are accompanied by rather dry conditions in all subregions. On the contrary, periods with low WT2 frequencies (e.g., the first half of the 1990s) are rather associated with positive precipitation anomalies. WT8 exhibits a frequency drop during the prolonged drought between 1999 and 2001, which has frequently been related to the simultaneous La Niña event (Barlow et al. 2002, 2016). The rather moist period between 1990 and 1995 is accompanied by an elevated frequency of WT7. While WT7 features highly variable relative frequencies between 5% and 25% before the mid-1990s, a frequency decrease is clearly depicted thereafter. A slight drying tendency during recent decades ($-0.51\%\,\mathrm{yr}^{-1}$ and $-1.63\%\,\mathrm{yr}^{-1}$ for subregions 2 and 3) is apparent in the observed and the reconstructed time series. It is noteworthy that the spatial pattern of precipitation trends (Fig. 13) is in close agreement with reconstructed trends, although the magnitude is distinctly reduced. This indicates that recent precipitation changes are partially controlled by a dynamic change of the regional circulation. Negative trends of cold season precipitation between 1980 and 2010 are characteristic for vast parts of central Asia. Positive trends are only observed along the Tian Shan and in southern Russia. The fact that the trend distribution roughly resembles the precipitation anomalies of WT7 (Fig. 11) supports the hypothesis that recent drying over central Asia is related to a reduced frequency of this pattern.

Although variations of ENSO have been shown to affect the frequency of WTs (section 3c), strong positive and negative deviations between observed and reconstructed precipitation anomalies are detected during El Niño (e.g., 1983, 1998, 2005, 2007; marked red in Fig. 13) and La Niña years (e.g., 1984, 1985, 1999–2001, 2008; marked blue). This finding suggests that the weather-type classification does not fully capture the influence of ENSO on the interannual variability of the tropical moisture supply from the Indian Ocean.

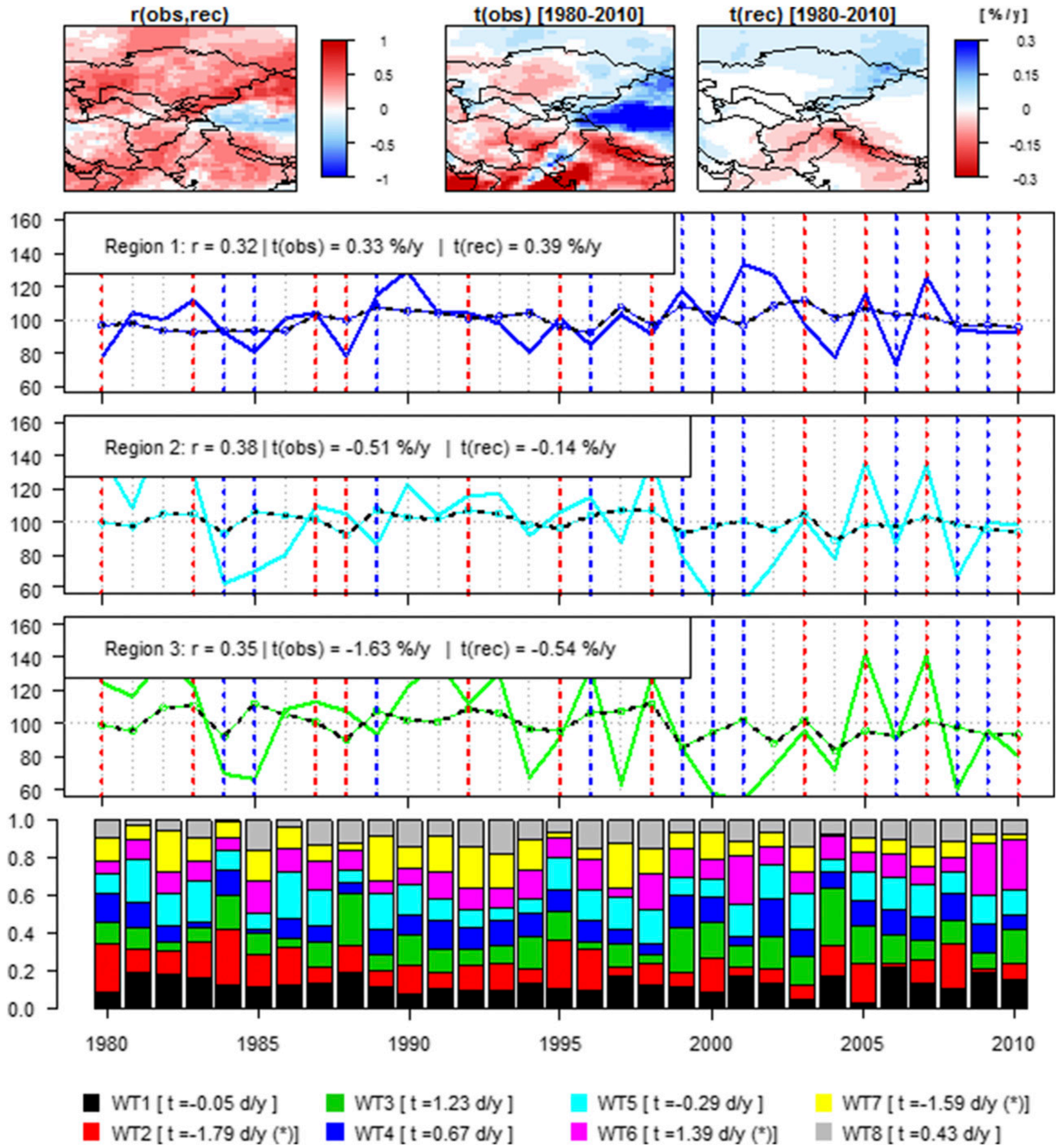

FIG. 13. (top) Spatial field of correlations between observed and WT-reconstructed seasonal precipitation sums *r*(obs,rec), *t*(obs), and *t*(rec) precipitation amounts for the extended winter seasons from 1979 to 2010. (middle) Line charts show the time series of observed and reconstructed precipitation anomalies (in percent of the seasonal mean precipitation sum) for each subregion. Red and blue verticals illustrate El Niño and La Niña events. Correlations between spatially averaged observations and reconstructions are depicted as well as observed and reconstructed precipitation trends. (bottom) The bar chart illustrates the time series of relative WT frequencies. Trends of seasonal WT frequencies (days yr^{-1}) are depicted and statistically significant trends are highlighted (*).

El Niño events are accompanied by an increase of SSTs over the western Indian Ocean (Terray and Dominiak 2005), which results in an amplification of evapotranspiration and thus in intensified moisture fluxes. The analysis of the WT internal precipitation variations for different quantiles of the seasonal Niño-3.4 index (Fig. 14) points toward a within-type influence of ENSO, that is, an alteration of the precipitation characteristics,

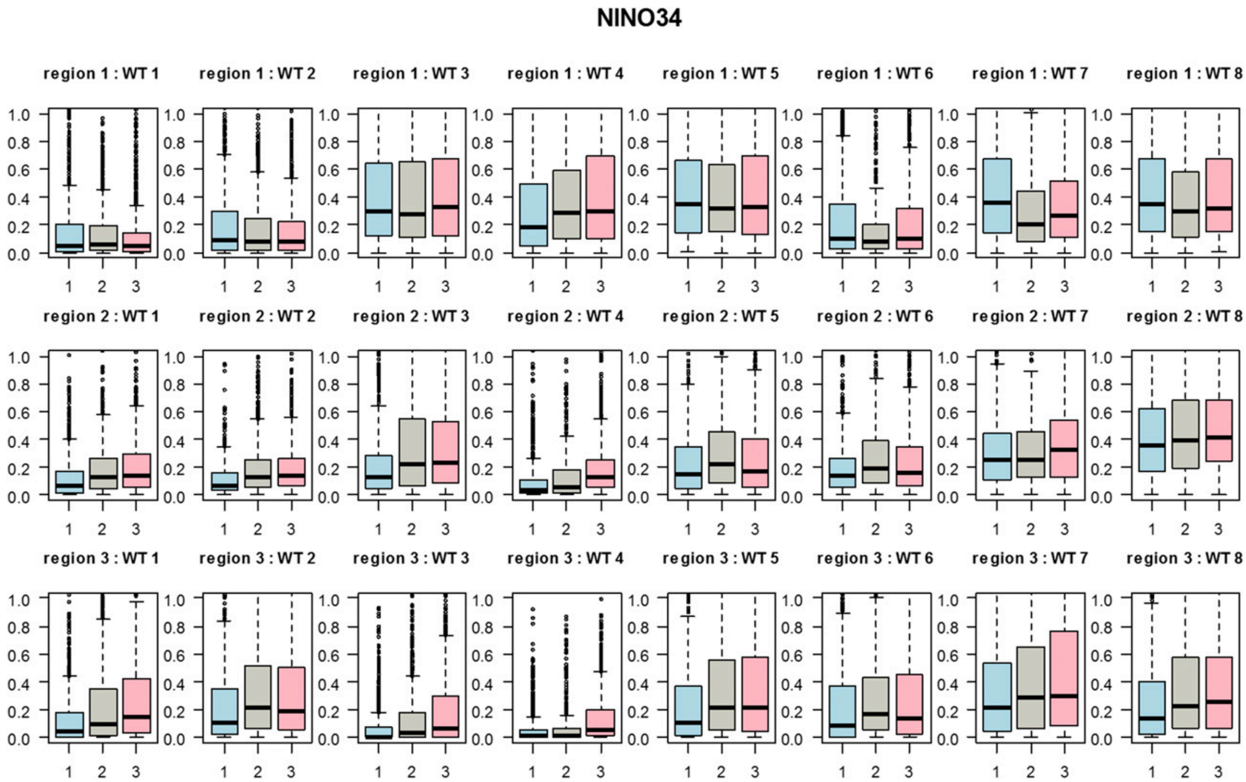

FIG. 14. Boxplots of spatially averaged 6-hourly precipitation (mm) for different WTs and central Asian subregions. The 6-hourly precipitation amounts are assigned to quantiles of the monthly Niño-3.4 index (1: La Niña, 0%–33% quantile; 2: neutral, 33%–66%; 3: El Niño, 66%–100%). Hinges represent the 25% and 75% quantile, whiskers are restricted to the 1.5-interquantile range, outliers are shown separately.

for each WT. Although the range of 6-hourly precipitation is large (with spatially averaged 6-hourly precipitation amounts between 0 and >0.5 mm), all WTs show a remarkable increase of precipitation during the El Niño phase for subregions 2 and 3. No clear WT internal influence is detected for Northern Hemispheric circulation indices (not shown).

4. Summary

In this study we investigate the cold season circulation patterns over central Asia by means of an objective weather-type classification analysis. The results give new insights into the regional climate conditions and their large-scale atmospheric drivers. Eight WTs were identified and analyzed in terms of their large-scale pressure patterns over Eurasia, their characteristic spell lengths and transitions, and their relations with remote teleconnections. Results indicate that central Asian WTs are strongly related with large-scale circulation modes over the Atlantic–European domain. Particularly the simultaneous positive manifestation of the Arctic Oscillation and the east Atlantic–western Russia pattern provokes WTs, associated with a planetary trough over central Asia and a consequential intensification of westerly moisture fluxes and cold air advection into the western target domain (WT3, WT7, and WT8). On the contrary, a negative EA/WR pattern favors WTs associated with a Rossby ridge over central Asia (WT1, WT2, and WT4), which implies a northward shift of westerly moisture fluxes and a suppression of precipitation. No significant relationship with NAO/AO has been detected for these WTs. Spatially asymmetrical Rossby tracks, associated with an intensified meridional flow over central Asia, are strongly related with variations of the Scandinavian pattern and modify the precipitation distribution with positive anomalies prevailing over the Tian Shan and rather negative anomalies over western parts of central Asia during its positive state (WT6). Likewise, temperature anomalies are linked to meridional flow components, with negative anomalies prevailing during the positive state of the Scandinavian pattern because of the northerly advection of polar air masses and positive anomalies during its negative phase, featuring mainly southerly winds. Besides Northern Hemispheric wave tracks, the regional circulation is strongly influenced by tropical circulation modes. In particular, a simultaneous El Niño is associated with an anticyclonic anomaly over northern India and an enhanced advection of moisture and heat from the Arabian Gulf and the Red Sea. Positive anomalies of sea surface temperatures over the western Indian Ocean further result in an increase of evapotranspiration and an enhanced moisture supply, which is manifested in a strong WT internal modification of precipitation characteristics during El Niño events.

In summary, WTs over central Asia have been interpreted as a superposition and regional manifestation of Northern Hemispheric wave patterns and tropical circulation modes. While the Northern Hemispheric contribution due to the propagation of Rossby waves is characterized by a high frequent variability and a short spell length of associated WTs, the ENSO-related influence is distinctly more persistent, and particularly WTs associated with the ENSO cold phase (WT2 and WT7) show a stationary behavior.

The variability of mean near-surface climate conditions at the seasonal scale has been shown to be captured by dynamic variations of the regional circulation as represented by the interannual variability of the WT composition. However, the skill of the purely dynamic WT classification in explaining seasonal climate anomalies depicts a distinct spatial variability and is significantly higher for temperature (with correlations in the order of $r = 0.8$) than for precipitation (up to $r = 0.4$). The exceptional high-temperature trends during the 1979–2010 period are shown to be assigned to variations of the WT composition by roughly 50%, indicating the important role of dynamical changes for central Asia, which has been previously identified as one of the hot spots of global warming (Giorgi 2006; Chen et al. 2009). Likewise, the spatial distribution of precipitation trends, displaying a slight drying tendency over the southern part of the target domain and rather positive trends over the Tian Shan and northern Kazakhstan, is captured by the WT analysis, although the trend magnitude is distinctly underestimated. Negative trends of seasonal WT frequencies have been detected for WT2 and WT7, which both feature negative pressure anomalies over the Indian Ocean and positive correlations with NAO/AO at the monthly scale. Thus, observed trends of dynamical circulation characteristics and consequential near-surface climate conditions are likely to be triggered by both tropical and extratropical mechanisms.

5. Discussion

The WTs over central Asia and their teleconnections with remote drivers emphasize the role of changing large-scale circulation characteristics for observed climatic trends during recent decades. A detailed investigation of changing circulation modes over the tropical oceans and the North Atlantic domain is thus required in order to understand the drivers of regional climate change and also to improve future climate change scenarios.

Positive trends of sea level pressure over the Indian Ocean during recent decades have been detected by Copsey et al. (2006), which is likely to be caused by altered SST conditions. While SST trends in the El Niño core region are marginal, strong positive trends have been detected in the western Pacific warm pool, resulting in an alteration of the Walker circulation (Sohn et al. 2013), which may modify the tropical fluxes of moisture and heat into the central Asian domain. Simultaneously, the Arctic/North Atlantic Oscillation experienced a negative shift during the 1990s, which has been shown to be linked with an increase of snow cover over the Eurasian continent and a decrease of sea ice in the polar oceans during autumn (Cohen et al. 2012; Handorf et al. 2015; Cohen and Entekhabi 1999). Liu et al. (2012) demonstrate that sea ice variations in the Arctic in summer and autumn influence the snow cover extent over Eurasia, particularly because of increased evapotranspiration during ice-free periods. Thus, the recent expansion of autumn snow cover over Eurasia and the consequential negative shift of AO might also be interpreted as a climate change signal, with strong implications for the central Asian climate.

Besides its skill in explaining observed trends of near-surface climate variables, the observed relationships of WT frequencies with large-scale climate modes might indicate a potential for an improvement of statistically based temperature and precipitation predictions at a seasonal scale, which is of great importance for the hydroclimatologically vulnerable target region. A profound understanding of cold season hydroclimatic variations, associated large-scale atmospheric processes, and their driving mechanisms is crucial in order to identify relevant predictor variables for seasonal predictions of water availability. While the influence of ENSO on the precipitation variability in central Asia is well acknowledged, little effort has yet been made to predict anomalous westerly moisture fluxes and related hydroclimatic variations in central Asia. Notwithstanding, various studies investigate the predictability of the large-scale Eurasian winter climate, particularly with regard to variations of the Arctic/North Atlantic Oscillation. Auspicious progress has been made by considering snow cover anomalies in October as a predictor for the mean state of AO during the subsequent winter (Cohen and Entekhabi 1999; Cohen et al. 2012). Both observational and modeling studies indicate that enhanced snow cover over Eurasia in October triggers an early and strong formation of the Siberian High, which results in an amplified jet stream and promotes the development of a negative AO (Allen and Zender 2011). Cohen and Jones (2011) illustrate that Eurasian snow cover in October serves as a skillful covariate for the prediction of winter temperature for large parts of the Northern Hemisphere. García-Serrano and Frankignoul (2014) and Brands et al. (2012) demonstrate the potential of statistically based winter precipitation forecasts for Europe taking cryospheric variables (i.e., snow cover and sea ice) over Eurasia and the Arctic during the preceding autumn as covariates. Further, SST anomalies in the Atlantic domain have been suggested as potential drivers of AO/NAO (Sutton et al. 2000; Czaja and Frankignoul 2002; Cassou et al. 2004) and the QBO has been identified as a potential predictor for the winter state of AO/NAO, with positive anomalies of QBO favoring the positive AO state (Boer and Hamilton 2008; Marshall and Scaife 2009). In a second part of the presented manuscript, we will investigate the skill of various tropical and extratropical predictor variables for the statistical forecast of cold season climate conditions in central Asia. With the aim of identifying the atmospheric mechanisms, allowing a robust forecast of seasonal climate anomalies, weather-type frequencies will be related with the state of tropical and extratropical drivers under consideration of selected lead times. Particularly the incorporation of autumn Eurasian snow cover is expected to improve state-of-the-art forecast models because of its effect on Northern Hemispheric planetary wave tracks and associated fluxes of moisture and heat into the central Asian domain.

Acknowledgments. This work was undertaken within the frame of the CAWa project (www.cawa-project.net) funded by the German Federal Foreign Office as part of the German Water Initiative for Central Asia (Grant AA7090002).

REFERENCES

Allen, R. J., and C. S. Zender, 2011: Forcing of the Arctic Oscillation by Eurasian snow cover. *J. Climate*, **24**, 6528–6539, https://doi.org/10.1175/2011JCLI4157.1.

Apel, H., and Coauthors, 2018: Statistical forecast of seasonal discharge in central Asia using observational records: Development of a generic linear modelling tool for operational water resource management. *Hydrol. Earth Syst. Sci.*, **22**, 2225–2254, https://doi.org/10.5194/hess-22-2225-2018.

Balsamo, G., and Coauthors, 2015: ERA-Interim/land: A global land surface reanalysis data set. *Hydrol. Earth Syst. Sci.*, **19**, 389–407, https://doi.org/10.5194/hess-19-389-2015.

Bao, X., and F. Zhang, 2013: Evaluation of NCEP–CFSR, NCEP–NCAR, ERA-Interim, and ERA-40 reanalysis datasets against independent sounding observations over the Tibetan Plateau. *J. Climate*, **26**, 206–214, https://doi.org/10.1175/JCLI-D-12-00056.1.

Barlow, M. A., and M. K. Tippett, 2008: Variability and predictability of central Asia river flows: Antecedent winter precipitation and large-scale teleconnections. *J. Hydrometeor.*, **9**, 1334–1349, https://doi.org/10.1175/2008JHM976.1.

——, and A. Hoell, 2015: Drought in the Middle East and central–southwest Asia during winter 2013/14 [in ''Explaining Extreme Events 2014'']. *Bull. Amer. Meteor. Soc.*, **96** (12), S71–S76, https://doi.org/10.1175/BAMS-D-15-00127.1.

——, H. Cullen, and B. Lyon, 2002: Drought in central and southwest Asia: La Niña, the warm pool, and Indian Ocean precipitation. *J. Climate*, **15**, 697–700, https://doi.org/10.1175/1520-0442(2002)015<0697:DICASA>2.0.CO;2.

——, B. Zaitchik, S. Paz, E. Black, J. Evans, and A. Hoell, 2016: A review of drought in the Middle East and Southwest Asia. *J. Climate*, **29**, 8547–8574, https://doi.org/10.1175/JCLI-D-13-00692.1.

Barnett, T. P., J. C. Adam, and D. P. Lettenmaier, 2005: Potential impacts of a warming climate on water availability in snow-dominated regions. *Nature*, **438**, 303–309, https://doi.org/10.1038/nature04141.

Bastos, A., and Coauthors, 2016: European land CO_2 sink influenced by NAO and east-Atlantic pattern coupling. *Nat. Commun.*, **7**, 10315, https://doi.org/10.1038/ncomms10315.

Bhandari, G., and B. B. Panthi, 2014: Analysis of agricultural drought and its effects on productivity at different district of Nepal. *J. Inst. Sci. Technol.*, **19**, 106–110, https://doi.org/10.3126/jist.v19i1.13835.

Boer, G. J., and K. Hamilton, 2008: QBO influence on extratropical predictive skill. *Climate Dyn.*, **31**, 987–1000, https://doi.org/10.1007/s00382-008-0379-5.

Bohner, J., 2006: General climatic controls and topoclimatic variations in central and high Asia. *Boreas*, **35**, 279–295, https://doi.org/10.1111/j.1502-3885.2006.tb01158.x.

Bothe, O., K. Fraedrich, and X. Zhu, 2012: Precipitation climate of central Asia and the large-scale atmospheric circulation. *Theor. Appl. Climatol.*, **108**, 345–354, https://doi.org/10.1007/s00704-011-0537-2.

Brands, S., R. Manzanas, J. M. Gutiérrez, and J. Cohen, 2012: Seasonal predictability of wintertime precipitation in Europe using the snow advance index. *J. Climate*, **25**, 4023–4028, https://doi.org/10.1175/JCLI-D-12-00083.1.

Bueh, C., and H. Nakamura, 2007: Scandinavian pattern and its climatic impact. *Quart. J. Roy. Meteor. Soc.*, **133**, 2117–2131, https://doi.org/10.1002/qj.173.

Cassou, C., L. Terray, J. W. Hurrell, and C. Deser, 2004: North Atlantic winter climate regimes: Spatial asymmetry, stationarity with time, and oceanic forcing. *J. Climate*, **17**, 1055–1068, https://doi.org/10.1175/1520-0442(2004)017<1055:NAWCRS>2.0.CO;2.

Chen, F., J. Wang, L. Jin, Q. Zhang, J. Li, and J. Chen, 2009: Rapid warming in mid-latitude central Asia for the past 100 years. *Front. Earth Sci. China*, **3**, 42–50, https://doi.org/10.1007/s11707-009-0013-9.

Cohen, J., and D. Entekhabi, 1999: Eurasian snow cover variability and Northern Hemisphere climate predictability. *Geophys. Res. Lett.*, **26**, 345–348, https://doi.org/10.1029/1998GL900321; Corrigendum, **26**, 1051, https://doi.org/10.1029/1999GL900200.

——, and J. Jones, 2011: A new index for more accurate winter predictions. *Geophys. Res. Lett.*, **38**, L21701, https://doi.org/10.1029/2011GL049626.

——, J. C. Furtado, M. A. Barlow, V. A. Alexeev, and J. E. Cherry, 2012: Arctic warming, increasing snow cover and widespread boreal winter cooling. *Environ. Res. Lett.*, **7**, 014007, https://doi.org/10.1088/1748-9326/7/1/014007.

Coleman, J. S. M., and J. C. Rogers, 2007: A synoptic climatology of the central United States and associations with Pacific teleconnection pattern frequency. *J. Climate*, **20**, 3485–3497, https://doi.org/10.1175/JCLI4201.1.

Copsey, D., R. Sutton, and J. R. Knight, 2006: Recent trends in sea level pressure in the Indian Ocean region. *Geophys. Res. Lett.*, **33**, L19712, https://doi.org/10.1029/2006GL027175.

Czaja, A., and C. Frankignoul, 2002: Observed impact of Atlantic SST anomalies on the North Atlantic Oscillation. *J. Climate*, **15**, 606–623, https://doi.org/10.1175/1520-0442(2002)015<0606:OIOASA>2.0.CO;2.

Dee, D. P., and Coauthors, 2011: The ERA-Interim reanalysis: Configuration and performance of the data assimilation system. *Quart. J. Roy. Meteor. Soc.*, **137**, 553–597, https://doi.org/10.1002/qj.828.

Diday, E., and J. C. Simon, 1980: Clustering analysis. *Digital Pattern Recognition*, K. S. Fu, Ed., Communication and Cybernetics, Vol. 10, Springer, 47–94.

Dimri, A. P., 2013: Interannual variability of Indian winter monsoon over the western Himalayas. *Global Planet. Change*, **106**, 39–50, https://doi.org/10.1016/j.gloplacha.2013.03.002.

Duethmann, D., and Coauthors, 2015: Attribution of streamflow trends in snow and glacier melt-dominated catchments of the Tarim River, central Asia. *Water Resour. Res.*, **51**, 4727–4750, https://doi.org/10.1002/2014WR016716.

El Kenawy, A. M, M. F. McCabe, G. L. Stenchikov, and J. Raj, 2014: Multi-decadal classification of synoptic weather types, observed trends and links to rainfall characteristics over Saudi Arabia. *Front. Environ. Sci.*, **2**, 37, https://doi.org/10.3389/fenvs.2014.00037.

García-Serrano, J., and C. Frankignoul, 2014: Retraction: High predictability of the winter Euro-Atlantic climate from cryospheric variability. *Nat. Geosci.*, **7**, E2, https://doi.org/10.1038/ngeo2164.

Gerlitz, L., O. Conrad, and J. Böhner, 2015: Large-scale atmospheric forcing and topographic modification of precipitation rates over high Asia—A neural-network-based approach. *Earth Syst. Dyn.*, **6**, 61–81, https://doi.org/10.5194/esd-6-61-2015.

——, S. Vorogushyn, H. Apel, A. Gafurov, K. Unger-Shayesteh, and B. Merz, 2016: A statistically based seasonal precipitation forecast model with automatic predictor selection and its application to central and south Asia. *Hydrol. Earth Syst. Sci.*, **20**, 4605–4623, https://doi.org/10.5194/hess-20-4605-2016.

Giorgi, F., 2006: Climate change hot-spots. *Geophys. Res. Lett.*, **33**, L08707, https://doi.org/10.1029/2006GL025734.

Golian, S., O. Mazdiyasni, and A. AghaKouchak, 2015: Trends in meteorological and agricultural droughts in Iran. *Theor. Appl. Climatol.*, **119**, 679–688, https://doi.org/10.1007/s00704-014-1139-6.

Handorf, D., R. Jaiser, K. Dethloff, A. Rinke, and J. Cohen, 2015: Impacts of Arctic sea ice and continental snow cover changes on atmospheric winter teleconnections. *Geophys. Res. Lett.*, **42**, 2367–2377, https://doi.org/10.1002/2015GL063203.

Hennig, C., 2007: Cluster-wise assessment of cluster stability. *Comput. Stat. Data Anal.*, **52**, 258–271, https://doi.org/10.1016/j.csda.2006.11.025.

Hoell, A., C. Funk, and M. Barlow, 2014: The regional forcing of Northern Hemisphere drought during recent warm tropical west Pacific Ocean La Niña events. *Climate Dyn.*, **42**, 3289–3311, https://doi.org/10.1007/s00382-013-1799-4.

Iglesias, I., M. N. Lorenzo, and J. J. Taboada, 2014: Seasonal predictability of the east Atlantic pattern from sea surface temperatures. *PLOS ONE*, **9**, e86439, https://doi.org/10.1371/journal.pone.0086439.

IPCC, 2013: *Climate Change 2013: The Physical Science Basis.* Cambridge University Press, 1535 pp., https://doi.org/10.1017/CBO9781107415324.

Krichak, S. O., and P. Alpert, 2005: Decadal trends in the east Atlantic–west Russia pattern and Mediterranean precipitation. *Int. J. Climatol.*, **25**, 183–192, https://doi.org/10.1002/joc.1124.

Lee, C. C., 2017: Reanalysing the impacts of atmospheric teleconnections on cold-season weather using multivariate surface weather types and self-organizing maps. *Int. J. Climatol.*, **37**, 3714–3730, https://doi.org/10.1002/joc.4950.

Liu, J., J. A. Curry, H. Wang, M. Song, and R. M. Horton, 2012: Impact of declining Arctic sea ice on winter snowfall. *Proc. Natl. Acad. Sci. USA*, **109**, 4074–4079, https://doi.org/10.1073/pnas.1114910109; Corrigendum, **109**, 6781–6783, https://doi.org/10.1073/pnas.1204582109.

Liu, W., L. Wang, D. Chen, K. Tu, C. Ruan, and Z. Hu, 2016: Large-scale circulation classification and its links to observed precipitation in the eastern and central Tibetan Plateau. *Climate Dyn.*, **46**, 3481–3497, https://doi.org/10.1007/s00382-015-2782-z.

Mariotti, A., 2007: How ENSO impacts precipitation in southwest central Asia. *Geophys. Res. Lett.*, **34**, L16706, https://doi.org/10.1029/2007GL030078.

Marshall, A. G., and A. A. Scaife, 2009: Impact of the QBO on surface winter climate. *J. Geophys. Res.*, **114**, D18110, https://doi.org/10.1029/2009JD011737.

Maussion, F., D. Scherer, T. Mölg, E. Collier, J. Curio, and R. Finkelnburg, 2014: Precipitation seasonality and variability over the Tibetan Plateau as resolved by the high Asia reanalysis. *J. Climate*, **27**, 1910–1927, https://doi.org/10.1175/JCLI-D-13-00282.1.

Michelangeli, P.-A., R. Vautard, and B. Legras, 1995: Weather regimes: Recurrence and quasi stationarity. *J. Atmos. Sci.*, **52**, 1237–1256, https://doi.org/10.1175/1520-0469(1995)052<1237:WRRAQS>2.0.CO;2.

Murawski, A., S. Vorogushyn, G. Bürger, L. Gerlitz, and B. Merz, 2018: Do changing weather types explain observed climatic trends in the Rhine basin? An analysis of within- and between-type changes. *J. Geophys. Res. Atmos.*, **123**, 1562–1584, https://doi.org/10.1002/2017JD026654.

Palazzi, E., J. von Hardenberg, and A. Provenzale, 2013: Precipitation in the Hindu-Kush Karakoram Himalaya: Observations and future scenarios. *J. Geophys. Res. Atmos.*, **118**, 85–100, https://doi.org/10.1029/2012JD018697.

Philipp, A., and Coauthors, 2010: Cost733cat—A database of weather and circulation type classifications. *Phys. Chem. Earth*, **35**, 360–373, https://doi.org/10.1016/j.pce.2009.12.010.

Roghani, R., S. Soltani, and H. Bashari, 2016: Influence of Southern Oscillation on autumn rainfall in Iran (1951–2011). *Theor. Appl. Climatol.*, **124**, 411–423, https://doi.org/10.1007/s00704-015-1423-0.

Roller, C. D., J.-H. Qian, L. Agel, M. Barlow, and V. Moron, 2016: Winter weather regimes in the Northeast United States. *J. Climate*, **29**, 2963–2980, https://doi.org/10.1175/JCLI-D-15-0274.1.

Schär, C., L. Vasilina, F. Pertziger, and S. Dirren, 2004: Seasonal runoff forecasting using precipitation from meteorological data assimilation systems. *J. Hydrometeor.*, **5**, 959–973, https://doi.org/10.1175/1525-7541(2004)005<0959:SRFUPF>2.0.CO;2.

Schiemann, R., D. Lüthi, P. L. Vidale, and C. Schär, 2008: The precipitation climate of central Asia—Intercomparison of observational and numerical data sources in a remote semiarid region. *Int. J. Climatol.*, **28**, 295–314, https://doi.org/10.1002/joc.1532.

——, ——, and C. Schär, 2009: Seasonality and interannual variability of the westerly jet in the Tibetan Plateau region. *J. Climate*, **22**, 2940–2957, https://doi.org/10.1175/2008JCLI2625.1.

Shepherd, T. G., 2014: Atmospheric circulation as a source of uncertainty in climate change projections. *Nat. Geosci.*, **7**, 703–708, https://doi.org/10.1038/ngeo2253.

Sheridan, S. C., 2003: North American weather-type frequency and teleconnection indices. *Int. J. Climatol.*, **23**, 27–45, https://doi.org/10.1002/joc.863.

Shirvani, A., and W. A. Landman, 2016: Seasonal precipitation forecast skill over Iran. *Int. J. Climatol.*, **36**, 1887–1900, https://doi.org/10.1002/joc.4467.

Smith, T. M., and R. W. Reynolds, 2003: Extended reconstruction of global sea surface temperatures based on COADS data (1854–1997). *J. Climate*, **16**, 1495–1510, https://doi.org/10.1175/1520-0442-16.10.1495.

Sohn, B. J., S.-W. Yeh, J. Schmetz, and H.-J. Song, 2013: Observational evidences of Walker circulation change over the last 30 years contrasting with GCM results. *Climate Dyn.*, **40**, 1721–1732, https://doi.org/10.1007/s00382-012-1484-z.

Sutton, R. T., W. A. Norton, and S. P. Jewson, 2000: The North Atlantic Oscillation—What role for the ocean? *Atmos. Sci. Lett.*, **1**, 89–100, https://doi.org/10.1006/asle.2000.0021.

Syed, F. S., F. Giorgi, J. S. Pal, and M. P. King, 2006: Effect of remote forcings on the winter precipitation of central southwest Asia. Part 1: Observations. *Theor. Appl. Climatol.*, **86**, 147–160, https://doi.org/10.1007/s00704-005-0217-1.

——, ——, ——, and K. Keay, 2010: Regional climate model simulation of winter climate over central–southwest Asia, with emphasis on NAO and ENSO effects. *Int. J. Climatol.*, **30**, 220–235, https://doi.org/10.1002/joc.1887.

Terray, P., and S. Dominiak, 2005: Indian Ocean sea surface temperature and El Niño–Southern Oscillation: A new perspective. *J. Climate*, **18**, 1351–1368, https://doi.org/10.1175/JCLI3338.1.

Trigo, R. M., C. M. Gouveia, and D. Barriopedro, 2010: The intense 2007–2009 drought in the Fertile Crescent: Impacts and associated atmospheric circulation. *Agric. For. Meteor.*, **150**, 1245–1257, https://doi.org/10.1016/j.agrformet.2010.05.006.

Wang, A., and X. Zeng, 2012: Evaluation of multireanalysis products with in situ observations over the Tibetan Plateau. *J. Geophys. Res.*, **117**, D05102, https://doi.org/10.1029/2011JD016553.

Wulf, H., B. Bookhagen, and D. Scherler, 2010: Seasonal precipitation gradients and their impact on fluvial sediment flux in the northwest Himalaya. *Geomorphology*, **118**, 13–21, https://doi.org/10.1016/j.geomorph.2009.12.003.

Yadav, R. K., J. H. Yoo, F. Kucharski, and M. A. Abid, 2010: Why is ENSO influencing northwest India winter precipitation in recent decades? *J. Climate*, **23**, 1979–1993, https://doi.org/10.1175/2009JCLI3202.1.

Yin, Z.-Y., H. Wang, and X. Liu, 2014: A comparative study on precipitation climatology and interannual variability in the lower midlatitude East Asia and central Asia. *J. Climate*, **27**, 7830–7848, https://doi.org/10.1175/JCLI-D-14-00052.1.